

BASIC RESEARCH PAPER

Mir143-BBC3 cascade reduces microglial survival via interplay between apoptosis and autophagy: Implications for methamphetamine-mediated neurotoxicity

Yuan Zhang^a, Kai Shen^a, Ying Bai^a, Xuan Lv^a, Rongrong Huang^a, Wei Zhang^a, Jie Chao^b, Lan K. Nguyen^{c,d}, Jun Hua^e, Guangming Gan^f, Gang Hu^e, and Honghong Yao^{a,g}

^aDepartment of Pharmacology, School of Medicine, Southeast University, Nanjing, Jiangsu, China; ^bDepartment of Physiology, School of Medicine, Southeast University, Nanjing, Jiangsu, China; ^cDepartment of Biochemistry and Molecular Biology, School of Biomedical Sciences, Monash University, Melbourne, Victoria Australia; ^dBiomedicine Discovery Institute, Monash University, Melbourne, Victoria Australia; ^eJiangsu Key Laboratory of Neurodegeneration, Department of Pharmacology, Nanjing Medical University, Nanjing, Jiangsu, China; ^fSchool of Medicine, Southeast University, Nanjing, Jiangsu, China; ^gInstitute of Life Sciences, Key Laboratory of Developmental Genes and Human Disease, Southeast University, Nanjing, Jiangsu, China

ABSTRACT

BBC3 (BCL2 binding component 3) is a known apoptosis inducer; however, its role in microglial survival remains poorly understood. In addition to the classical transcription factor TRP53, *Mir143* is involved in BBC3 expression at the post-transcriptional level. Here, we identify unique roles of *Mir143*-BBC3 in mediating microglial survival via the regulation of the interplay between apoptosis and autophagy. Autophagy inhibition accelerated methamphetamine-induced apoptosis, whereas autophagy induction attenuated the decrease in microglial survival. Moreover, *anti-Mir143*-dependent BBC3 upregulation reversed the methamphetamine-induced decrease in microglial survival via the regulation of apoptosis and autophagy. The *in vivo* relevance of these findings was confirmed in mouse models, which demonstrated that the microinjection of *anti-Mir143* into the hippocampus ameliorated the methamphetamine-induced decrease in microglia as well as that observed in heterozygous *Mir143*^{+/-} mice. These findings provide new insight regarding the specific contributions of *Mir143*-BBC3 to microglial survival in the context of drug abuse.

ARTICLE HISTORY

Received 18 September 2015
Revised 10 May 2016
Accepted 16 May 2016

KEYWORDS

apoptosis; autophagy; BBC3; methamphetamine; microglia; *Mir143*

Introduction

Methamphetamine abuse is a major social and health concern. Methamphetamine is a popular addictive pharmacological psychostimulant of the central nervous system (CNS), and its use is associated with multiple neuropsychiatric adverse reactions as well as neurotoxicity to the dopaminergic and serotonergic systems of the brain.^{1,2} Methamphetamine-induced neurotoxicity is associated with microglial activation that is thought to participate in either pro-toxic or protective mechanisms in the brain. Microglia, CNS cells of the myeloid lineage, play an important role in immune surveillance and compromised microglial function is associated with various neurological pathologies.^{3,4}

Accumulating evidence suggests that microglia might also be activated during the process of methamphetamine-induced toxicity in animals.⁵⁻⁹ A previous study indicated that chronic methamphetamine abuse is also associated with microglial activation in the brains of human methamphetamine addicts.¹⁰ Activated microglia eventually undergo apoptosis by a process known as activation-induced cell death (AICD). Activated microglia secrete not only neurotrophic factors, thereby prolonging neuronal survival, but also cytotoxic mediators, such as

nitric oxide (NO), and cytokines, such as TNF and IL1B, that induce inflammation and neurotoxicity. Cytotoxic factors such as NO and pro-inflammatory cytokines that are secreted from activated microglia have been shown to mediate AICD through the regulation of apoptotic proteins, including caspases and the BCL2 family of proteins.¹¹ Although methamphetamine is known to induce microglial activation, whether methamphetamine induces AICD in microglia and the molecular mechanisms in this process remains elusive.

BBC3/PUMA (BCL2 binding component 3) is an essential apoptosis inducer. BBC3 is one of the most common apoptosis inducers among the BCL2-homology 3 (BH3)-only subgroup of BCL2 family members.^{12,13} BBC3 is transcriptionally activated by a wide range of apoptotic stimuli and transduces proximal death signals to the mitochondria. BBC3 directly binds to all 5 known anti-apoptotic BCL2 family members with high affinities through its BH3 domain. The binding of BBC3 to the BCL2-like proteins results in the displacement of BAX-BAK1 and the activation of these proteins via the formation of multimeric pore-like structures on the mitochondrial outer membrane, leading to mitochondrial dysfunction and caspase activation. BBC3 is implicated in many pathological and

CONTACT Honghong Yao  yaohh@seu.edu.cn  Department of Pharmacology, School of Medicine, Southeast University Dingjiaqiao 87, Nanjing, Jiangsu, China 210009; Gang Hu  ghu@njmu.edu.cn

Color versions of one or more of the figures in the article can be found online at www.tandfonline.com/kaup.

 Supplemental data for this article can be accessed on the publisher's website.

physiological processes, including cancer, tissue injury, neurodegenerative diseases, immune response and bacterial or viral infections.¹⁴ Although the function of BBC3 in apoptosis has been extensively illustrated in different tissues, whether BBC3 is involved in methamphetamine-induced microglial apoptosis remains poorly understood.

BBC3 was initially identified as a transcriptional target of TP53 and as a mediator of DNA damage-induced apoptosis;^{15,16} however, the regulation of *Bbc3* expression by noncoding RNAs in microglia has not yet been explored. Computational algorithms such as TargetScan were employed to identify the microRNAs (miRs) that target evolutionarily conserved sequences in the *Bbc3* gene. *Mir143*, which is conserved among vertebrates, was predicted to target *Bbc3*. miRs are small, evolutionarily conserved noncoding RNAs that are derived from substantially larger primary transcripts. Recent studies have demonstrated that miRs expressed by immune cells can target proteins that regulate inflammation and consequently affect the magnitude of the immune response.¹⁷ miRs are becoming increasingly recognized as important regulators of cell functions, including glial activation.¹⁷⁻²³ *Mir143* has a well-established role in the differentiation and proliferation of bovine intramuscular preadipocytes.²⁴ Moreover, *Mir143* decreases cell growth by targeting SDC1 (syndecan1) in melanoma²⁵ as well as in colon tumor cells.²⁶ Jordan et al. demonstrated that obesity-induced *Mir143* overexpression (OE) inhibits insulin-stimulated AKT1/Akt activation and impairs glucose metabolism.²⁷ However, the role of *Mir143* in mediating microglial survival remains unexplored.

Our study revealed an unexpected function of BBC3 that was regulated by *Mir143* at the post-transcriptional level via the regulation of the interplay between autophagy and apoptosis, which contradicts its known role as an essential apoptosis inducer. These findings provide the first evidence that the *Mir143*-BBC3 axis mediates a regulatory pathway critical for the regulation of microglial survival. Specific blockage of *Mir143* could be a potential therapeutic target for treating decreased microglial survival in the context of drug abuse and other neurodegenerative diseases.

Results

Paradoxical role of BBC3 in reduced microglial survival induced by methamphetamine

Although BBC3 has been intensively studied for many years, its role in the viability of microglia treated with methamphetamine has remained elusive. As an initial screen to better understand how methamphetamine affects microglial survival, we examined the effect of methamphetamine on microglial survival in various brain regions in mice. As shown in Fig. S1A, unlike in the striatum and cortex, administration of methamphetamine significantly decreased the number of microglial cells in the hippocampus, as evidenced by the finding that the expression of the microglial marker-AIF1/Iba-1 (allograft inflammatory factor 1) in the hippocampus was significantly decreased compared with the saline control group. Therefore, the hippocampus was chosen as the region of interest for our *in vivo* study. Because BBC3 functions as an essential apoptosis inducer, we

hypothesized that BBC3 deficiency might attenuate methamphetamine-induced cell death. As shown in Fig. 1A and B, methamphetamine administration significantly decreased the number of AIF1-positive cells in the hippocampus. Surprisingly, BBC3 deficiency further decreased the number of microglia in the presence of methamphetamine instead of reversing the methamphetamine-induced decrease in microglia cell number, contradicting the known role of BBC3 as an apoptosis inducer (Fig. 1A and B).

Activated microglia eventually undergo apoptosis by a process termed AICD; however, whether methamphetamine causes AICD of microglia remains largely unknown. Therefore, we first examined the effect of methamphetamine on cell viability. BV-2 cells were exposed to different concentrations of methamphetamine (15 μ M, 150 μ M and 1.5 mM), and cell viability was assessed. The rationale for choosing these concentrations was based on the concentration of methamphetamine in the postmortem brains of chronic abusers.^{28,29} As shown in Fig. S2A, 1.5 mM methamphetamine decreased BV-2 cell viability as determined by Cell Counting Kit-8 (CCK8) assay. Therefore, this concentration of methamphetamine was chosen for all further studies. To address whether methamphetamine-induced cell death is due to mitochondria-dependent mechanisms, the cytosolic and mitochondrial CYCS (cytochrome c, somatic) levels were determined. As shown in Fig. S2B and C, methamphetamine treatment of BV-2 cells increased the CYCS level in the cytosol (Fig. S2B) and decreased the CYCS level in the mitochondrial fraction (Fig. S2C). We next explored whether methamphetamine-induced cell death also involved alterations in mitochondrial membrane potential. Cells were exposed to methamphetamine for different periods (6, 12, and 24 h), and then mitochondrial membrane depolarization was assessed using the JC-1 probe, which is a fluorescent lipophilic cationic dye that accumulates in mitochondria in proportion to the membrane potential that normally exists across the inner mitochondrial membrane. As shown in Fig. S2D and E, methamphetamine treatment increased the ratio of JC-1 aggregate: JC-1 monomer as determined using both a microscope (Fig. S2D) and a plate reader (Fig. S2E). Taken together, these data indicated that methamphetamine-induced cell death is related to mitochondria.

Studies have shown that nitric oxide (NO) is involved in LPS-induced AICD.^{30,31} Therefore, we next investigated the effect of methamphetamine on the expression of NOS2/iNOS (nitric oxide synthase 2, inducible). As shown in Fig. S3A, methamphetamine significantly increased NOS2 expression, with a peak response at 1 h. Pretreatment of cells with the NOS2 inhibitor-nitro-L-arginine methyl ester (L-NAME) attenuated methamphetamine-induced cell death (Fig. S3B). Consistent with this *in vitro* finding, administration of another NOS2 inhibitor, aminoguanidine (75 mg/kg), for 5 consecutive d followed by the administration of methamphetamine attenuated the methamphetamine-induced decrease in microglia as determined by Western blot for AIF1 expression in the hippocampus (Fig. S3C and D).

Next, we dissected the role of BBC3 in methamphetamine-induced microglial survival. Lentiviral vector-transduced *Bbc3* siRNA in BV-2 cells successfully decreased BBC3 expression as shown in Fig. 1C (upper panel). Methamphetamine

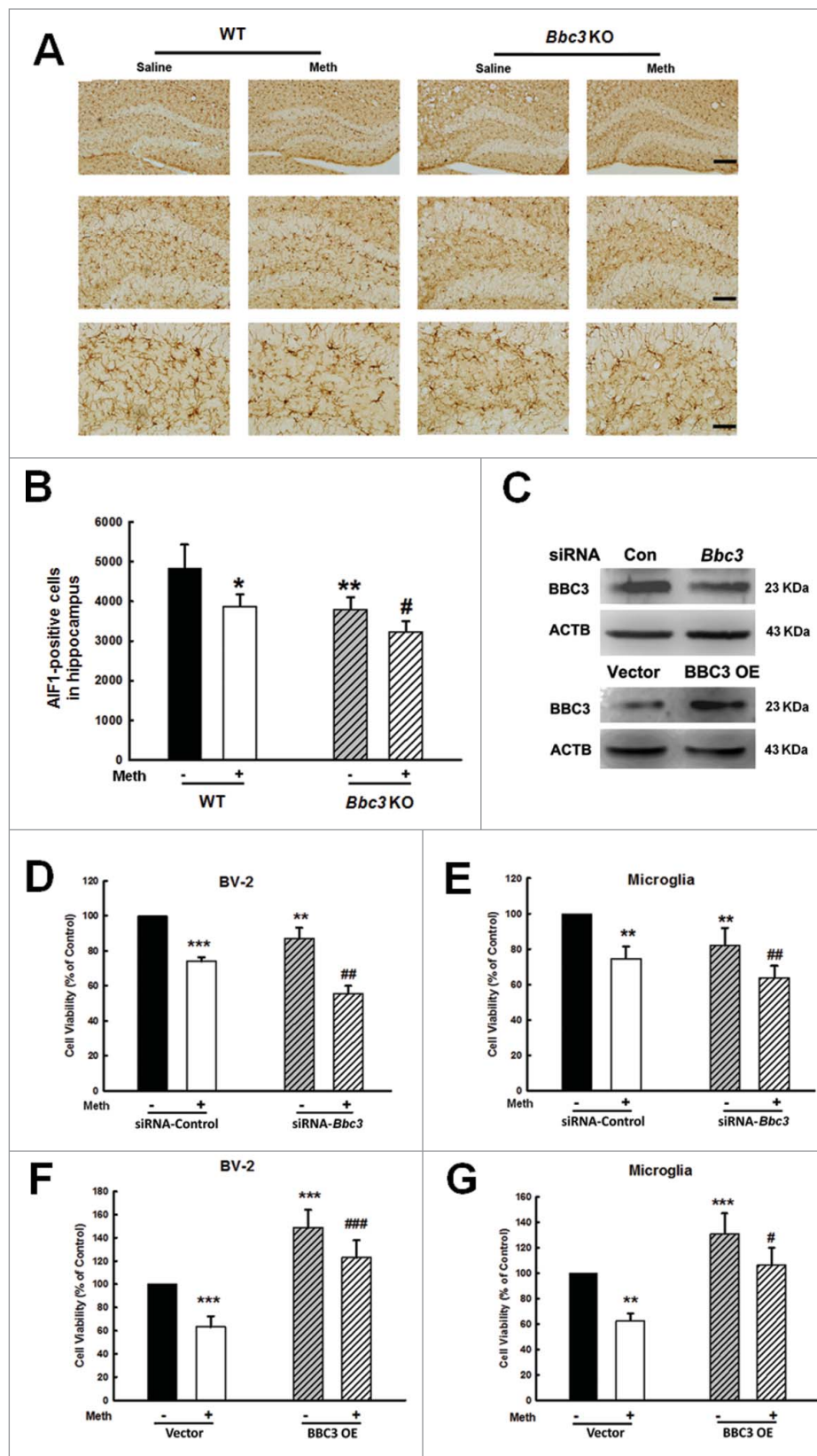


Figure 1. Paradoxical role of BBC3 in the methamphetamine-induced decrease in microglial survival. (A) The effect of methamphetamine on the survival of microglia in the hippocampus of WT and *Bbc3* KO mice. WT and *Bbc3* KO mice were treated with methamphetamine (intraperitoneal, 30 mg/kg) for 48 h, followed by AIF1 immunostaining. Representative image of AIF1 immunostaining in the hippocampus of mice injected with saline/methamphetamine. Scale bars: 200 μ m (upper panel), 100 μ m (middle panel), and 50 μ m (lower panel). (B) Stereology of AIF1-positive microglia in the hippocampus. $N = 6$ animals/group. *, $p < 0.05$, **, $p < 0.01$ vs. the saline-treated group; #, $p < 0.05$ vs. the methamphetamine-treated group using one-way ANOVA followed by the Holm-Sidak test. (C) *Bbc3* siRNA lentivirus was transduced to decrease BBC3 expression (upper panel), and the cells were transduced with BBC3 OE lentivirus to increase BBC3 expression (lower panel). (D and E) Transduction of cells with *Bbc3* siRNA lentivirus failed to ameliorate the decreased microglial survival as assessed by CCK8 assay in both BV-2 cells (D) and primary mouse microglia (E). (F and G) Transduction of cells with a BBC3 OE lentivirus ameliorated the decreased microglial survival as assessed by CCK8 in both BV-2 cells (F) and primary mouse microglia (G). All data are given as the mean \pm SD of 3 independent experiments. **, $p < 0.01$ and ***, $p < 0.001$ vs. the siRNA-control or vector group; #, $p < 0.05$, ##, $p < 0.01$ and ###, $p < 0.001$ vs. the methamphetamine-treated group using one-way ANOVA followed by the Holm-Sidak test. Meth, methamphetamine.

significantly decreased the survival of BV-2 cells (Fig. 1D) as well as in primary mouse microglia (Fig. 1E), whereas *Bbc3* knockdown using siRNA significantly decreased cell viability and aggravated the methamphetamine-induced decrease in microglial survival. To further confirm the role of BBC3 in microglial survival, cells were transduced with BBC3 OE lentivirus. As shown in Fig. 1F and G, transduction of cells with BBC3 OE lentivirus successfully increased BBC3 expression (Fig. 1C, lower panel) and significantly attenuated the methamphetamine-induced decrease in cell survival in both BV-2 cells (Fig. 1F) and primary mouse microglia (Fig. 1G).

To further confirm our findings, we next examined the role of BBC3 in cell viability using trypan blue dye exclusion assay, as shown in Fig. S4. Methamphetamine treatment increased the number of trypan blue-positive cells; *BBC3* knockdown using siRNA further increased the number of trypan blue-positive cells. However, BBC3 OE significantly inhibited the increase in trypan blue-positive cells compared with the methamphetamine-treated group.

Methamphetamine-mediated upregulation of BBC3 in microglia at the transcriptional level

BBC3 plays a seemingly paradoxical role in microglia in vivo and in vitro studies; however, very little is known regarding the detailed mechanisms underlying BBC3 expression in methamphetamine-induced AICD of microglia. Therefore, we examined the effect of methamphetamine on BBC3 expression. BV-2 cells were exposed to methamphetamine for various periods. Compared with the control group, *Bbc3* mRNA was significantly upregulated as determined by real-time PCR (Fig. 2A and B). Having determined that methamphetamine increased BBC3 expression at the mRNA level, we next confirmed the increase in BBC3 expression by western blot analysis. Exposure to methamphetamine resulted in a biphasic response with an early but significant and transient increase in BBC3 (Fig. 2C, 6 h) followed by later significant repression of BBC3 (Fig. 2C, 24 h). To further confirm the effect of methamphetamine on BBC3 expression, primary mouse microglia were treated with methamphetamine (Fig. 2D). Consistent with the finding in BV-2 cells, methamphetamine treatment induced sustained expression of *Bbc3* at the mRNA level but dynamic BBC3 expression at the protein level (Fig. 2B and D). The methamphetamine-mediated regulation of BBC3 expression was further validated by immunostaining (Fig. 2E). Taken together, these data clearly demonstrated that methamphetamine mediated the induction of BBC3 expression in microglia.

While methamphetamine induced BBC3 expression, *Bbc3* mRNA and protein expression patterns were inconsistent. This inconsistency may be due to the co-regulation of BBC3 expression at the transcriptional and post-transcriptional levels. BBC3 was initially identified as a transcriptional target of TP53 (TRP53 in mice) and a mediator of DNA damage-induced apoptosis; our study also indicated that methamphetamine treatment triggered the translocation of TRP53 into the nucleus (Fig. 2F, left panel) in a time-dependent manner without significant effect on the level of TRP53 in the cytosolic fraction (Fig. 2F, middle panel). Interestingly, methamphetamine treatment increased the expression of TRP53 in the total cell lysates (Fig. 2F, right panel). Moreover,

blockage of the TRP53 pathway using a TRP53 inhibitor and *Trp53*-specific siRNA significantly decreased BBC3 expression in primary mouse microglia (Fig. 2G and H). As expected, *Trp53* siRNA successfully decreased TRP53 expression in primary mouse microglia (Fig. S5). Therefore, the transcription factor TRP53 was involved in methamphetamine-induced BBC3.

Mir143 regulates BBC3 expression in microglia at the post-transcriptional level

Intriguingly, methamphetamine treatment induced a transient increase in the BBC3 protein levels before it decreased to a level comparable to that in the control group, despite a sustained increase in *Bbc3* expression at the mRNA level (Fig. 2A to D). This result strongly suggested that an additional mechanism exists that negatively regulates BBC3 protein expression likely at the post-transcriptional level. Therefore, we further examined the detailed mechanisms of this process. We determined that BBC3 was regulated by the transcription factor TRP53 in microglia cells; however, whether BBC3 expression is regulated by noncoding RNAs has not previously been explored in microglia. The next step was to examine the miR that targets BBC3 using the TargetScan algorithm. Computational algorithms such as TargetScan were employed, and *Mir143*, which is conserved among vertebrates, was predicted to target *Bbc3*.

As shown in Fig. 3A, *Bbc3* has a conserved *Mir143* binding site within its 3'-untranslated region (UTR) in most species that was identified as the putative target of *Mir143*. Intriguingly, cotransfecting a *Mir143*-overexpressing vector and the pmir-GLO plasmid with the *Bbc3* wild type 3'-UTR resulted in the downregulation of luciferase activity, and this effect was reversed in H293 cells transfected with a mutated *Bbc3* 3'-UTR (Fig. 3B). The next step was to determine whether methamphetamine mediated its effects via the induction of *Mir143* and to assess the kinetics of the methamphetamine response. Methamphetamine treatment of primary mouse microglia induced a biphasic response resulting in early but significant and transient repression of *Mir143* (Fig. 3C; 6h) that was followed by later but sustained and significant upregulation of *Mir143* (Fig. 3C; 24 h). Interestingly and as expected, methamphetamine-induced modulation of *Mir143* correlated inversely with BBC3 expression (Fig. 2C and D). Methamphetamine-mediated regulation of *Mir143* was further validated using fluorescence in situ hybridization (FISH; Fig. 3D). In line with this finding, *Mir143* decreased BBC3 expression, whereas *anti-Mir143* increased BBC3 expression at both the mRNA (Fig. 3E) and protein (Fig. 3F) levels in primary mouse microglia.

Role of BBC3 in methamphetamine-induced apoptosis of microglia

Because BBC3 expression was increased in the BV-2 cells in the presence of methamphetamine, we next sought to explore the role of BBC3 in the methamphetamine-mediated apoptosis of BV-2 cells. As shown in Fig. 4A to C, methamphetamine induced the expression of BAX, but failed to affect the levels of BCL2L1/Bcl-xL, cleaved CASP9 (caspase 9) and cleaved CASP3. Moreover, knockdown of *Bbc3* using *Bbc3*-specific siRNA alleviated the expression of methamphetamine-

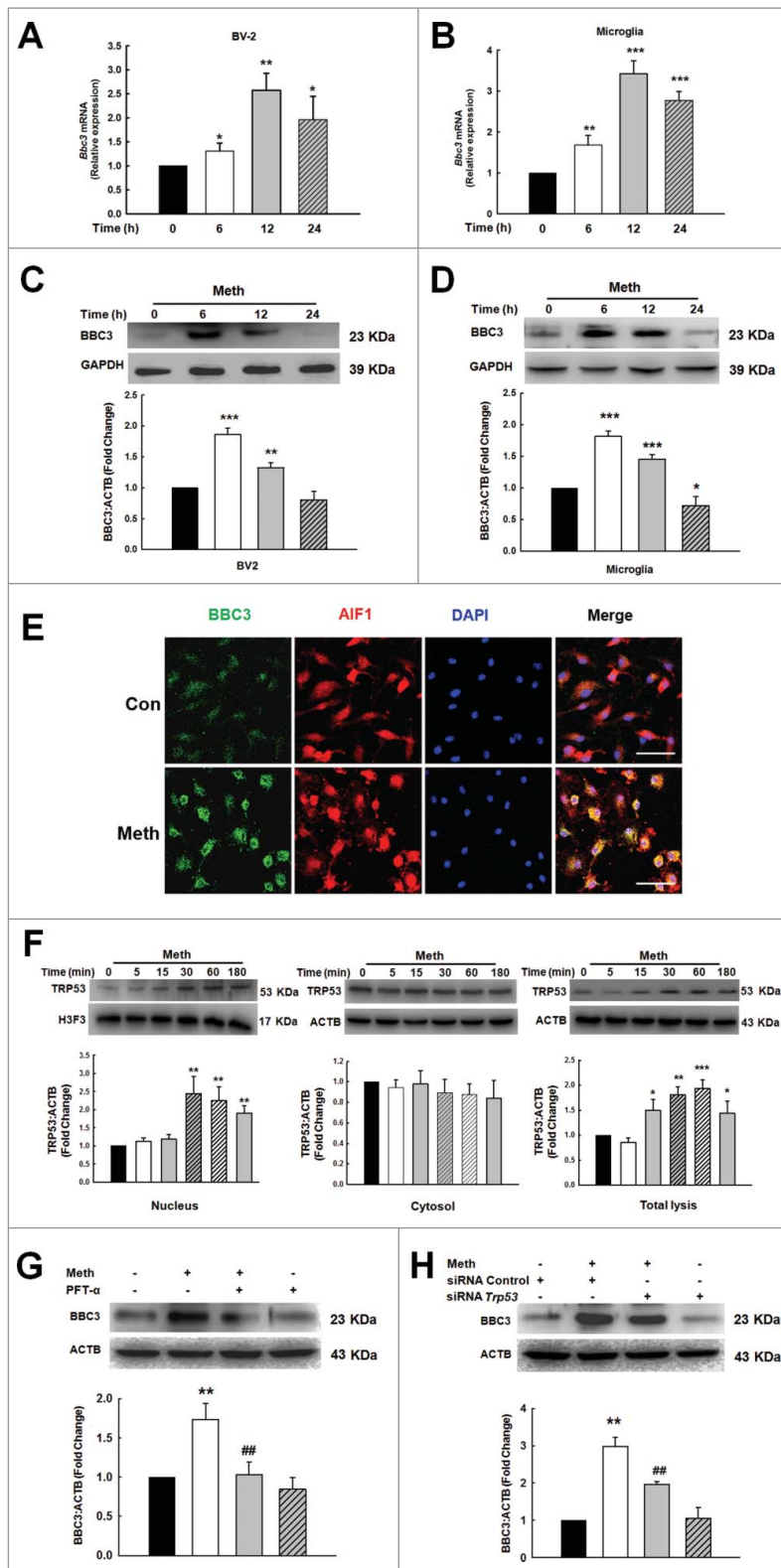


Figure 2. Methamphetamine mediated upregulation of BBC3 in microglia. (A and B) Methamphetamine increased *Bbc3* expression at the mRNA level in BV-2 cells (A) and in primary mouse microglia (B) as determined by real-time PCR. (C and D) Methamphetamine induced a biphasic response of BBC3 expression in BV-2 cells (C) and in primary mouse microglia (D) as determined by western blot analysis. Cells were treated with methamphetamine (1.5 mM) for 6, 12 and 24 h, followed by collection of RNA and protein for assessment of BBC3 expression. All data are presented as the mean \pm SD of 3 independent experiments. *, $p < 0.05$, **, $p < 0.01$ and ***, $p < 0.001$ vs. the control group using one-way ANOVA followed by the Holm-Sidak test. (E) Representative image of BBC3 immunofluorescence staining in primary mouse microglia. Cells were treated with methamphetamine (1.5 mM) for 6 h. Red, AIF1; green, BBC3; blue, DAPI. Scale bar: 50 μ m. (F) Methamphetamine increased TRP53 expression and induced TRP53 translocation into the nuclei of BV-2 cells. Cells were treated with methamphetamine for 5, 15, 30, 60 and 180 min followed by isolation of nuclear and cytosolic fractions as well as collection of the total cell lysates for the detection of TRP53 expression using western blot analysis. All data are presented as the mean \pm SD of 3 independent experiments. *, $p < 0.05$, **, $p < 0.01$ and ***, $p < 0.001$ vs. the control group using one-way ANOVA followed by the Holm-Sidak test. (G and H) Pretreatment of primary mouse microglia with the TRP53 inhibitor pifithrin- α (PFT- α ; 10 μ M) for 1 h (G) or *Trp53* siRNA (H), followed by treatment with methamphetamine for 6 h. Inhibition of the TRP53 pathway significantly decreased the BBC3 expression induced by methamphetamine. All data are presented as the mean \pm SD of 3 independent experiments. **, $p < 0.01$ vs. the control group; ##, $p < 0.01$ vs. the methamphetamine-treated group using one-way ANOVA followed by the Holm-Sidak test. Meth, methamphetamine.

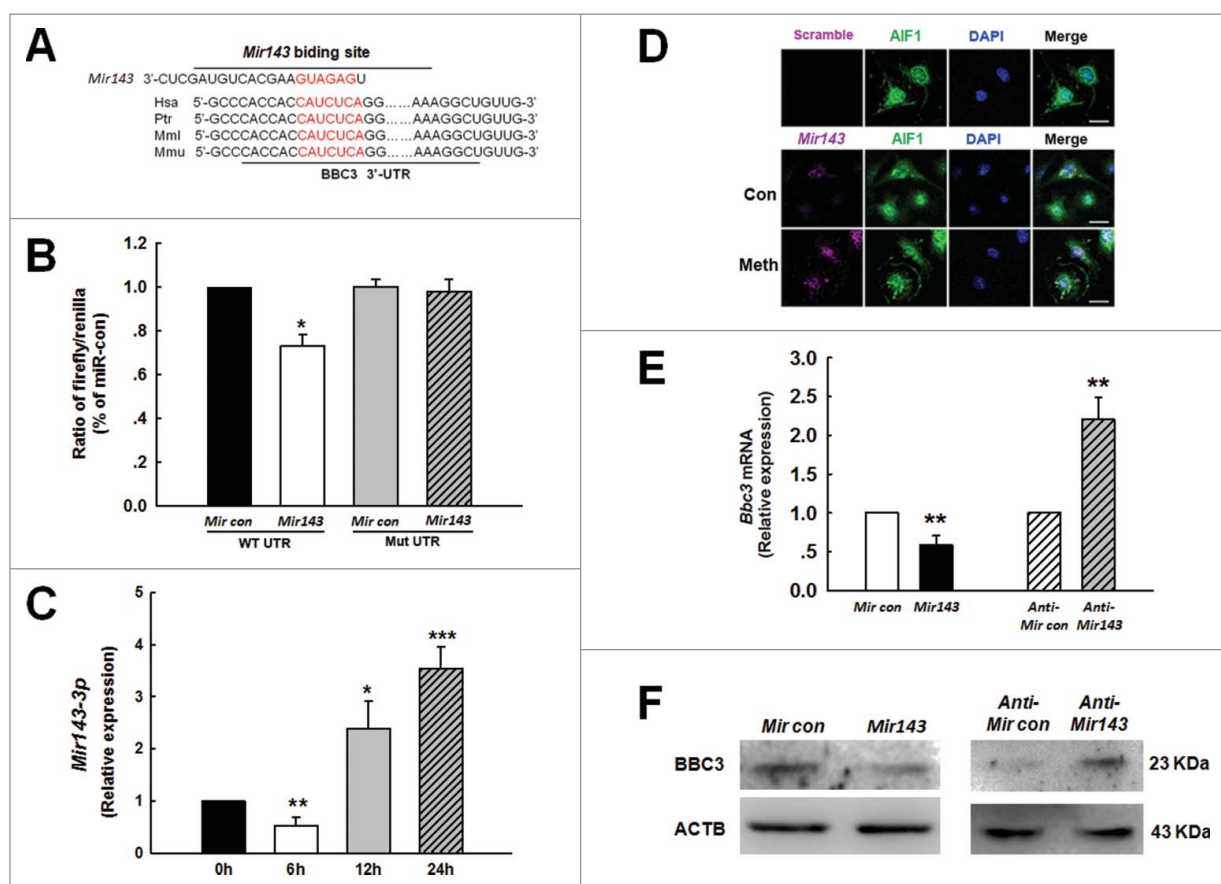


Figure 3. *Mir143* regulates *BBC3* expression at the post-transcriptional level in microglia. (A) Putative *Mir143* binding sites in the *Bbc3* gene. The potential complementary residues are shown in red. (B) Relative luciferase activity of wild type 3'-UTR mutant constructs of *Bbc3* cotransfected with the *Mir143* OE vector and the pmir-GLO plasmid. All the data are indicated as the mean \pm SD of 3 individual experiments. *, $p < 0.05$ vs. the *Mircontrol* co-transfected with WT group using one-way ANOVA followed by the Holm-Sidak test. (C) Effect of methamphetamine on *Mir143* expression at the mRNA level in primary mouse microglia as determined by real-time PCR. Cells were incubated with methamphetamine (1.5 mM) for 6, 12 and 24 h, followed by collection of RNA for assay of *Mir143* expression. All data are presented as the mean \pm SD of 3 independent experiments. *, $p < 0.05$; **, $p < 0.01$; and ***, $p < 0.001$ vs. the control group using one-way ANOVA followed by the Holm-Sidak test. (D) Fluorescence in situ hybridization of mature *Mir143* in primary mouse microglia combined with immunostaining for the microglial marker AIF1. Cells were incubated with methamphetamine (1.5 mM) for 24 h. Red, *Mir143*; green, AIF1; blue, DAPI. Scale bar: 20 μ m. (E and F) Primary mouse microglia infected with *Mircontrol* + *Mir143* and *anti-Mircontrol* + *anti-Mir143* lentivirus for 48 h were assessed for *BBC3* expression at the mRNA (E) and protein (F) levels. All data are presented as the mean \pm SD of 3 individual experiments. **, $p < 0.01$ vs. the *Mircontrol* or *anti-Mircontrol* group using Student *t* test. Meth, methamphetamine.

mediated markers of apoptosis (Fig. 4D to F). To corroborate the above findings, terminal deoxynucleotidyl transferase-mediated dUTP nick end-labeling (TUNEL) staining was performed, which demonstrated that 25.8% of cells treated with methamphetamine were TUNEL-positive and that this increase in cell apoptosis was significantly reduced in the cells transduced with *Bbc3* siRNA (Fig. 4G and H). To further confirm the role of *BBC3* in microglial apoptosis, the effect of methamphetamine on cleaved CASP9 and cleaved CASP3 was examined in primary mouse microglia. As shown in Fig. 5A and B, methamphetamine increased the levels of cleaved CASP9 and cleaved CASP3. Moreover, knockdown of *BBC3* expression significantly inhibited the increase in cleaved CASP3 induced by methamphetamine (Fig. 5C). Because *BBC3* is a common apoptosis inducer, we next examined the effect of *BBC3* efficiency on cell apoptosis in vivo. As shown in Fig. 5D and E, methamphetamine-mediated upregulation of BAX-BCL2L1 and cleaved CASP3 was ameliorated in the hippocampus of *Bbc3* knockout (KO) mice compared with WT controls. Taken together, these findings suggested that *BBC3* is involved in methamphetamine-mediated apoptosis.

Role of *BBC3* in methamphetamine-induced autophagy of microglia

To explain the paradoxical role of *BBC3* in microglial survival, we investigated whether *BBC3* affected autophagy, a critical regulatory process of cell survival and proliferation.³² Two well-known pathways are involved in autophagy: the phosphoinositide 3-kinase-AKT1-MTOR-RPS6KB signaling pathway and the RAS-RAF1-MAPK1/2 signaling pathway. Both pathways are often activated in numerous types of cancers.³³ Several anticancer agents are known to inhibit the phosphoinositide 3-kinase-AKT1-MTOR-RPS6KB signaling pathway and to simultaneously activate the MAPK1/ERK2 pathway, resulting in autophagy induction.³⁴⁻³⁶ Therefore, we first examined the effect of methamphetamine on these pathways. As shown in Fig. S6, methamphetamine treatment suppressed the phosphorylation of AKT1, MTOR, and RPS6K but increased the phosphorylation of MAPK1. Next, we examined MAP1LC3-II/LC3-II expression in the presence of methamphetamine. As shown in Figure 6A and B, methamphetamine treatment of both BV-2 and primary mouse microglia increased the expression of

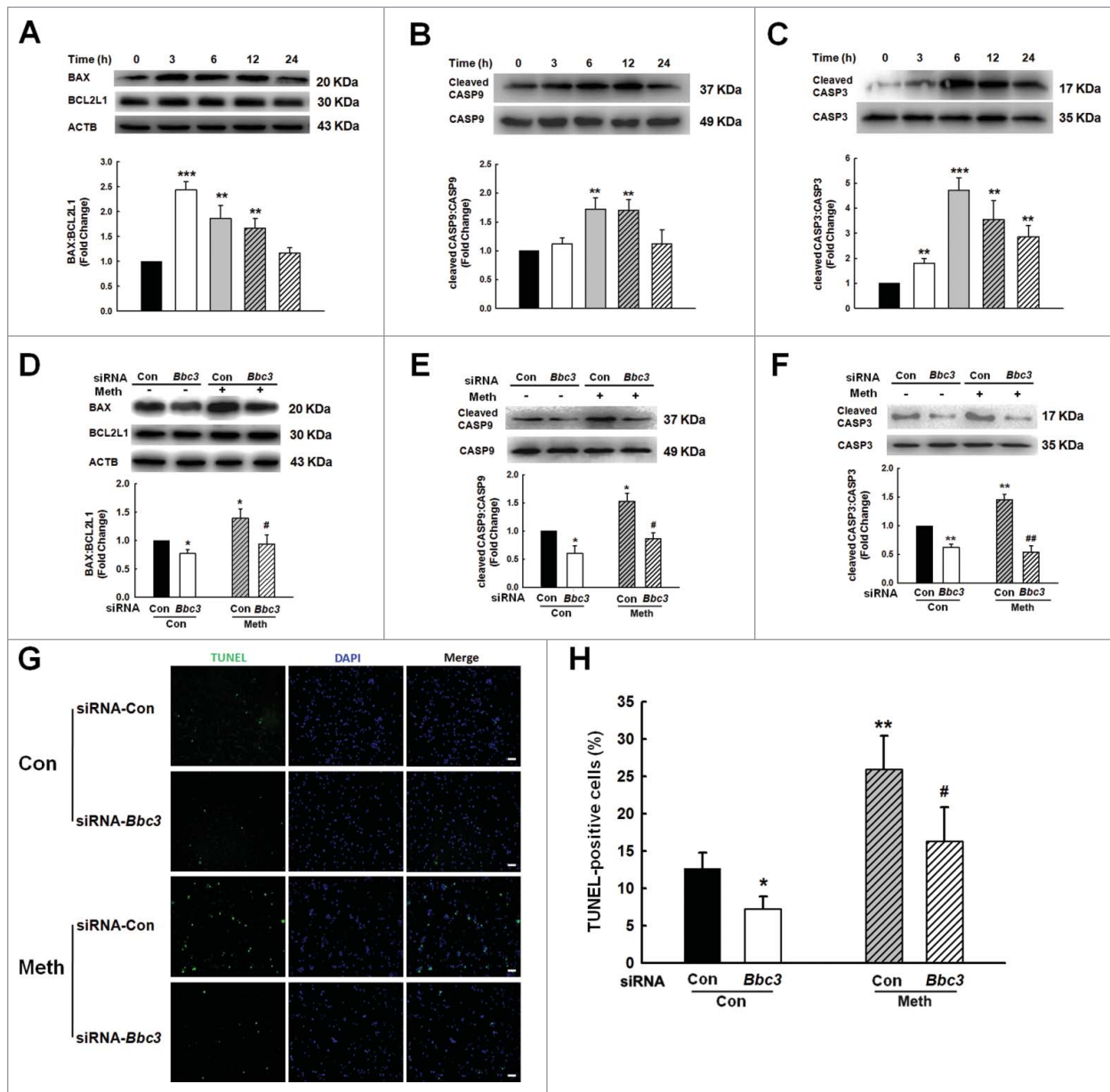


Figure 4. Role of BBC3 in methamphetamine-induced cell apoptosis of BV-2 cells. (A to C) Exposure of BV-2 cells to methamphetamine (1.5 mM) for different time periods (3, 6, 12 and 24 h) increased the expression of BAX-BCL2L1 (A), cleaved CASP9:CAP9 (B) and cleaved CASP3:CAP3 (C). All data are presented as the mean \pm SD of 3 independent experiments. **, $p < 0.01$ and ***, $p < 0.001$ vs. the control group using one-way ANOVA followed by the Holm-Sidak test. (D to F) Methamphetamine-induced expression of BAX-BCL2L1 (D), cleaved CASP9:CAP9 (E) and cleaved CASP3:CAP3 (F) was attenuated by BBC3 knockdown in BV-2 cells using *Bbc3* siRNA in BV-2 cells. BV-2 cells were transfected with *Bbc3* siRNA for 24 h followed by methamphetamine treatment (1.5 mM) for another 6 h, and the cells were homogenized for detection of cleaved CASP9 and CASP3 expression using western blotting. (G and H) TUNEL staining (green) in BV-2 cells transfected with *Bbc3* siRNA for 24 h and treated with methamphetamine for another 24 h. All data are presented as the mean \pm SD of 3 independent experiments. *, $p < 0.05$ and **, $p < 0.01$ vs. the control group; #, $p < 0.05$ and ##, $p < 0.01$ vs. the methamphetamine-treated group using one-way ANOVA followed by the Holm-Sidak test.

BECN1/Beclin 1 and induced the production of MAP1LC3-II, which is a cleaved MAP1LC3-phosphatidylethanolamine conjugate and a general autophagosomal marker.³⁷ In the context of autophagy, SQSTM1/p62 acts as a receptor protein that links MAP1LC3 with ubiquitin moieties on misfolded proteins. Therefore, autophagy mediates the clearance of SQSTM1 together with ubiquitinated proteins. Consistently, SQSTM1 expression was downregulated by methamphetamine treatment in both BV-2 and primary mouse microglia (Fig. 6A and B).

Autophagic flux was further monitored in primary mouse microglia that were transduced with tandem fluorescent-mRFP-GFP-MAP1LC3-adenovirus, a specific marker for

autophagosome formation that relies on the different nature of GFP and RFP fluorescence under acidic conditions. GFP fluorescence is sensitive to the acidic condition of the lysosome lumen, while RFP is relatively stable under acidic conditions. Thus, the colocalization of GFP and RFP signals (yellow dots) indicates the phagophores or autophagosomes that have not fused with lysosomes, whereas RFP-only signals (red puncta) stain the autolysosomes. As shown in Fig. 6C, methamphetamine treatment significantly increased the number of yellow dots per cell with a concomitant greater increase in RFP-only MAP1LC3 dots in primary mouse microglia transduced with tandem fluorescent-tagged nRFP-GFP-MAP1LC3. Autophagy

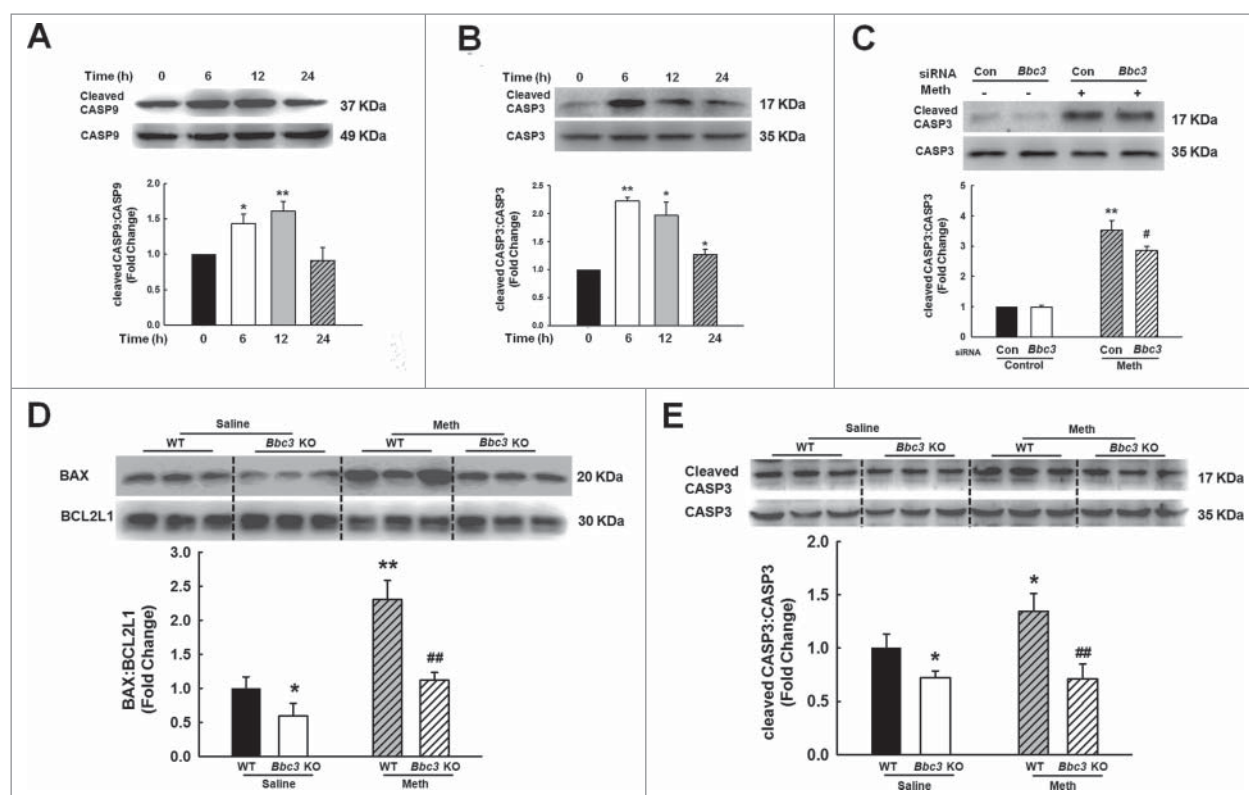


Figure 5. Role of BBC3 in methamphetamine-induced microglial apoptosis. (A and B) Exposure of primary mouse microglia to methamphetamine (1.5 mM) for different time periods (6, 12 and 24 h) increased the expression of cleaved CASP9 and CASP3. All data are presented as the mean \pm SD of 3 independent experiments. *, $p < 0.05$ and **, $p < 0.01$ vs. the control group using one-way ANOVA followed by the Holm-Sidak test. (C) *Bbc3* siRNA inhibited the methamphetamine-induced increase in cleaved CASP3 expression. Primary mouse microglia were transduced with *Bbc3* siRNA for 24 h followed by methamphetamine treatment (1.5 mM) for another 6 h, and the cells were homogenized for detection of cleaved CASP3 expression using western blotting. All data are presented as the mean \pm SD of 3 independent experiments. **, $p < 0.01$ vs. the control group; #, $p < 0.05$ vs. the methamphetamine-treated group using one-way ANOVA followed by the Holm-Sidak test. (D and E) Expression of BAX-BCL2L1 (D) and cleaved CASP3:CASP3 (E) in the hippocampus of WT and *Bbc3* KO mice as determined by western blotting. WT and *Bbc3* KO mice were treated with methamphetamine (intraperitoneal, 30 mg/kg) for 48 h followed by examination for apoptosis. $N = 6$ animals/group. *, $p < 0.05$ and **, $p < 0.01$ vs. the saline-treated WT group; ##, $p < 0.01$ vs. the methamphetamine-treated WT group using one-way ANOVA followed by the Holm-Sidak test. Meth: methamphetamine.

is a dynamic process of protein degradation that is characterized by the formation of double-membraned cytoplasmic vesicles.³⁸ Structural analysis via electron microscopy allows the visualization of autophagy with the massive accumulation of autophagic vacuoles (autophagosomes) and autolysosomes in the cytoplasm. As shown in Fig. 6D, methamphetamine treatment resulted in the accumulation of numerous autolysosomes (arrow) and double-membraned autophagic vacuoles (arrowhead) in primary microglia (Fig. S7).

Because MAP1LC3-II can be increased by either enhanced autophagy initiation or inhibition of lysosomal degradation,³⁹ we next examined the mechanisms underlying the methamphetamine-induced increase in MAP1LC3-II expression. BV-2 cells were pretreated with the lysosome inhibitors bafilomycin A₁ (BafA1) and chloroquine (CQ) for 1 h followed by methamphetamine treatment for 24 h. The cells were then collected, and homogenates were prepared for detection of MAP1LC3-II levels. As shown in Fig. 7, methamphetamine increased the level of MAP1LC3-II in the presence of CQ (Fig. 7A and C) or BafA1 (Fig. 7B and D) compared with BV-2 cells (Fig. 7A and B) and primary mouse microglia (Fig. 7C and D) treated with CQ or BafA1 alone, suggesting that methamphetamine increased MAP1LC3-II levels primarily through enhancing autophagy initiation.

The anti-apoptotic protein BCL2 binds with BECN1 to inhibit the autophagic process, and a previous study demonstrated that methamphetamine treatment resulted in disruption of the interaction between BCL2 and BECN1.⁴⁰ To determine whether such a mechanism was also responsible for methamphetamine-induced autophagy, we investigated the binding status of BCL2 with BECN1 following methamphetamine treatment. Using co-immunoprecipitation assays, the amount of BECN1 in the BCL2-immunoprecipitated protein complex was shown to decrease while the amount of total BCL2 remained unchanged in methamphetamine-treated microglia, as shown in Fig. S8.

Our findings demonstrated that the change in the levels of MAP1LC3-II occurred at 24 h following methamphetamine treatment (Fig. 6), when BBC3 expression had already returned to the basal level (Fig. 2). According to this finding, the role of autophagy as a mechanism of BBC3-mediated cell survival seems to be confusing considering the timing of these events. However, as shown in Fig. 6A, methamphetamine treatment resulted in the increased expression of BECN1 as early as 6 h, which is consistent with the response of BBC3; methamphetamine induced a transient increase in the BBC3 protein level at 6 h followed by reduction to a level comparable to that of the control group (Fig. 2). BECN1 is an adaptor protein that

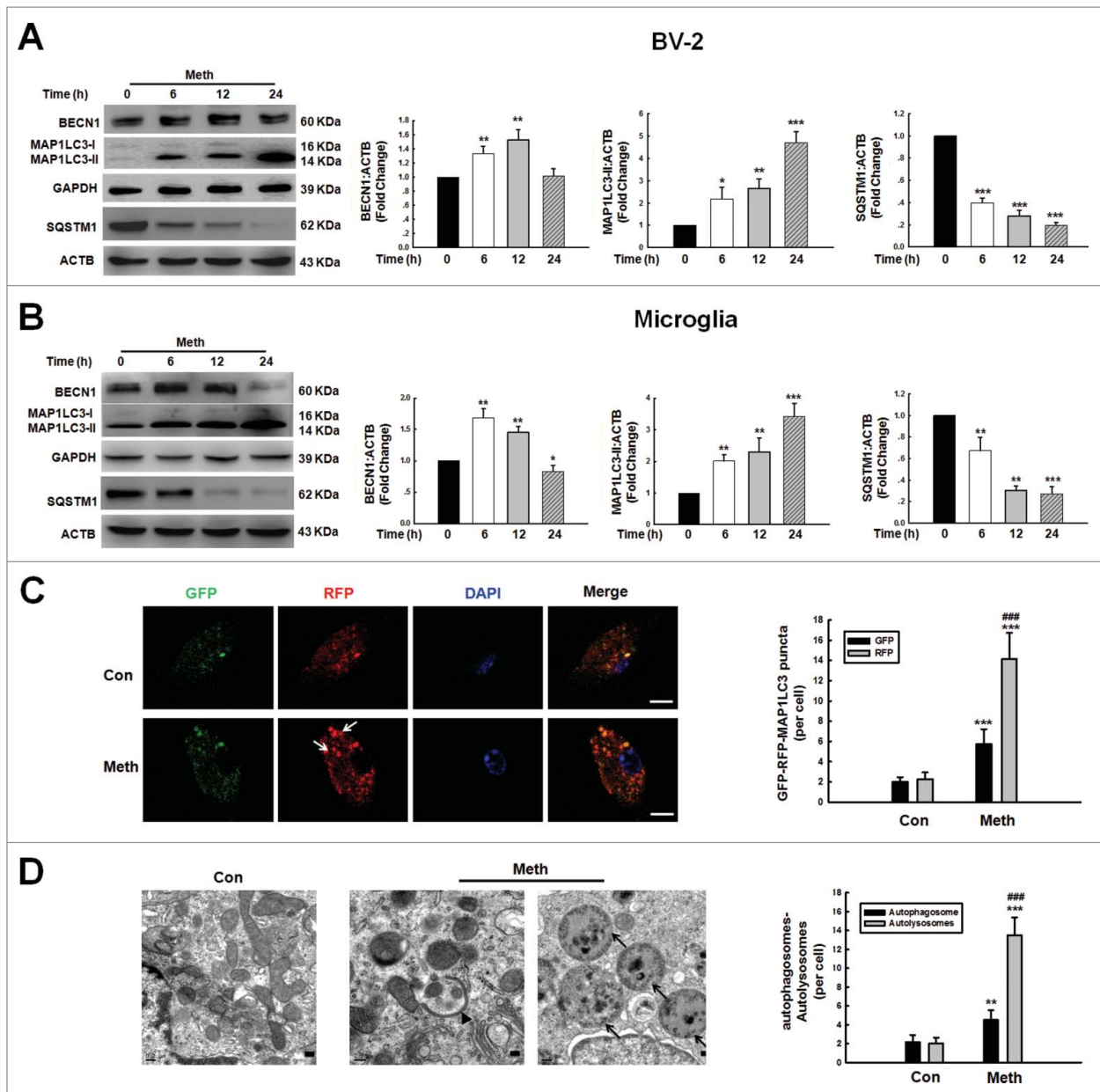


Figure 6. Methamphetamine induced microglial autophagy. (A and B) The expression of BECN1, MAP1LC3-II and SQSTM1 in BV-2 cells (A) and primary mouse microglia (B) induced by methamphetamine. Cells were treated with methamphetamine (1.5 mM) for 6, 12 and 24 h. All data are presented as the mean \pm SD of 3 independent experiments. *, $p < 0.05$; **, $p < 0.01$; and ***, $p < 0.001$ vs. the control group using one-way ANOVA followed by the Holm-Sidak test. (C) Primary mouse microglia infected with RFP-GFP-MAP1LC3 adenovirus and then treated with 1.5 mM methamphetamine for 24 h. Effect of methamphetamine on RFP- and GFP-MAP1LC3 puncta (left panel). Scale bar: 5 μ m. The RFP- and GFP-MAP1LC3 puncta per cell were counted, and the quantification is shown in the right panel. (D) Transmission electron microscopy imaging of cells showing autolysosomes (arrows) and double-membraned autophagosomes (arrowheads) in primary microglia (left panel) and quantification of autolysosomes and autophagosomes (right panel) in primary microglial cells treated with methamphetamine (1.5 mM) for 24 h. Scale bar: 200 nm. Quantification of cell numbers is presented as the mean \pm SD of 3 independent experiments. **, $p < 0.01$ and ***, $p < 0.001$ vs. the control group; ###, $p < 0.01$ vs. the methamphetamine-treated group using one-way ANOVA followed by the Holm-Sidak test.

assembles a core complex with phosphatidylinositol 3-kinase to recruit other autophagy-related proteins that orchestrate autophagosome formation and thus plays a central role in autophagy induction.⁴⁰⁻⁴² Therefore, our current finding suggested that the early increase in BECN1 expression could initiate autophagy by increasing the level of BECN1 and that BECN1 expression further initiated the process of autophagy in a dynamic, time-dependent manner. To confirm this possibility, BV-2 cells were transfected with *Bbc3* siRNA followed by treatment with methamphetamine. As shown in Fig. S9A, knockdown of BECN1 expression significantly inhibited

methamphetamine-induced BECN1 expression. Moreover, we also demonstrated that BECN1 knockdown significantly diminished MAP1LC3-II expression, thus indicating that BECN1 lies upstream of MAP1LC3-II (Fig. S9B). As expected, BECN1 siRNA successfully decreased BECN1 expression as shown in Fig. S9C.

MAP1LC3-II formation was enhanced by the autophagy inducer rapamycin, as shown in Fig. 8A and B. This effect was also confirmed by immunofluorescence staining showing that rapamycin enhanced the number of vacuoles as indicated by endogenous MAP1LC3-II (Fig. 8A and B). Having determined

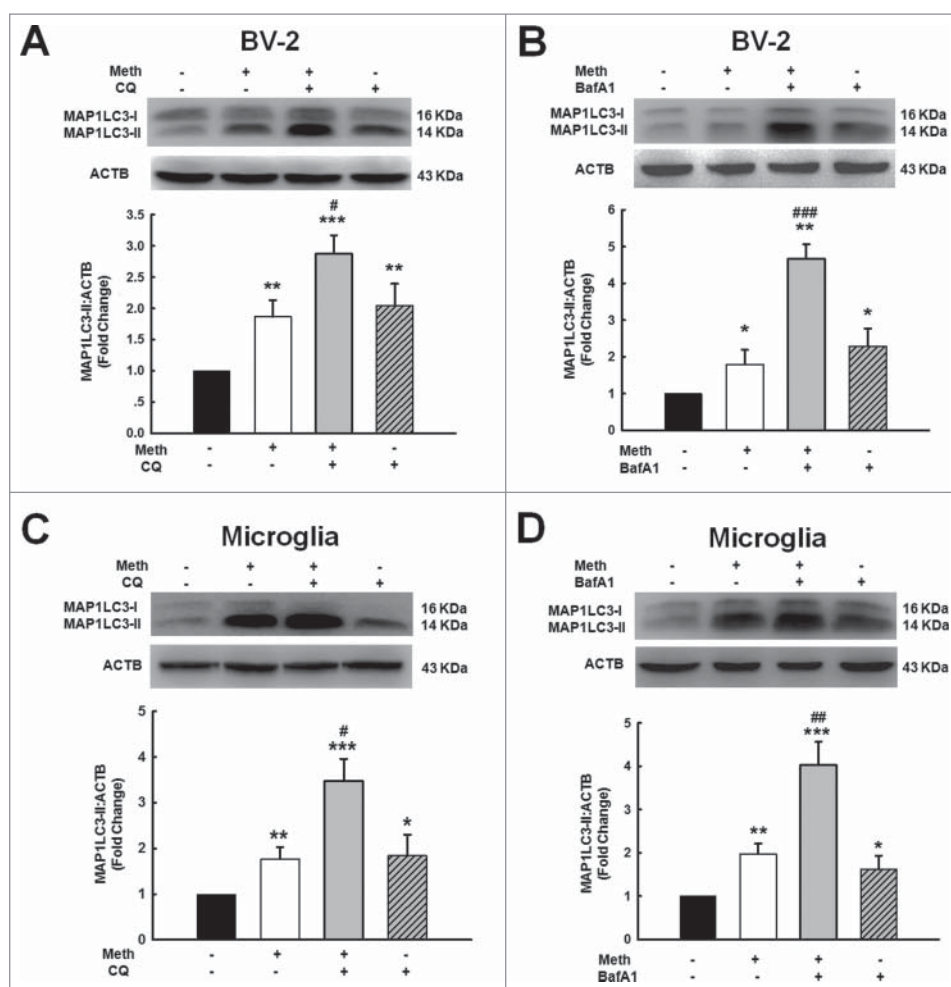


Figure 7. Methamphetamine increased MAP1LC3-II level primarily through enhancing the initiation of autophagy. (A and B) BV-2 cells were pretreated with or without CQ (45 μ M) (A) or BafA1 (50 nM) (B) for 1 h followed by methamphetamine (1.5 mM) treatment for 24 h. (C and D) primary mouse microglia were pretreated with or without CQ (45 μ M) (C) or BafA1 (50 nM) (D) for 1 h followed by methamphetamine (1.5 mM) treatment for 24 h. All data are presented as the mean \pm SD of 3 independent experiments. *, $p < 0.05$, **, $p < 0.01$ and ***, $p < 0.001$ vs. the control group; #, $p < 0.05$, ##, $p < 0.01$ and ###, $p < 0.01$ vs. the CQ- or BafA1-treated group using one-way ANOVA followed by the Holm-Sidak test. Meth, methamphetamine; CQ, chloroquine; BafA1, bafilomycin A₁.

that methamphetamine induced BBC3 expression and autophagy, we next sought to explore the role of BBC3 in methamphetamine-mediated autophagy. As shown in Fig. 8C, transduction of primary mouse microglia with a lentiviral vector carrying *Bbc3* siRNA significantly reversed methamphetamine-induced MAP1LC3-II expression. In contrast, BBC3 OE further enhanced the methamphetamine-induced increase in MAP1LC3-II expression (Fig. 8D). Furthermore, the level of MAP1LC3-II was significantly increased in WT mice treated with methamphetamine, and this level was reduced in the *Bbc3* KO mice (Fig. 8E). Taken together, these findings suggested that BBC3 plays a critical role in methamphetamine-induced autophagy.

Role of autophagy in the methamphetamine-induced decrease in cell viability

The finding that BBC3 is required for microglial survival, as shown in Fig. 1, was unexpected as these data contradicted the common view that BBC3 is an essential apoptosis inducer. Because BBC3 was involved in methamphetamine-induced autophagy and because autophagy is considered to have a

prosurvival role under pathological conditions, we next determined the role of autophagy in the survival of microglia treated with methamphetamine. Primary mouse microglia were treated with the autophagy inhibitor 3-methyladenine (3-MA), which is a class III phosphatidylinositol 3-kinase inhibitor that prevents autophagy at an early stage of autophagosome formation. As shown in Fig. 9A, pretreatment of cells with 3-MA enhanced the methamphetamine-induced decrease in cell viability. 3-MA alone had no effect on cell viability. However, pretreatment of cells with the autophagy inducer rapamycin significantly ameliorated the methamphetamine-induced decrease in cell viability (Fig. 9B) suggesting that autophagy exerted a prosurvival role in microglia, whereas the inhibition of autophagy decreased cell viability. In order to confirm the role of autophagy in methamphetamine-induced decreased cell viability of microglia, cells were transduced with siRNA *Atg7* (autophagy-related 7) lentivirus. As shown in Fig. 9C and D, knockdown of ATG7 further decreased microglial survival in both BV-2 and primary mouse microglia. As expected, lentiviral vector-transduced *Atg7* siRNA significantly decreased ATG7 expression in primary mouse microglia and enhanced BAX-BCL2L1 expression, as shown in Fig. S10. To further confirm the role of

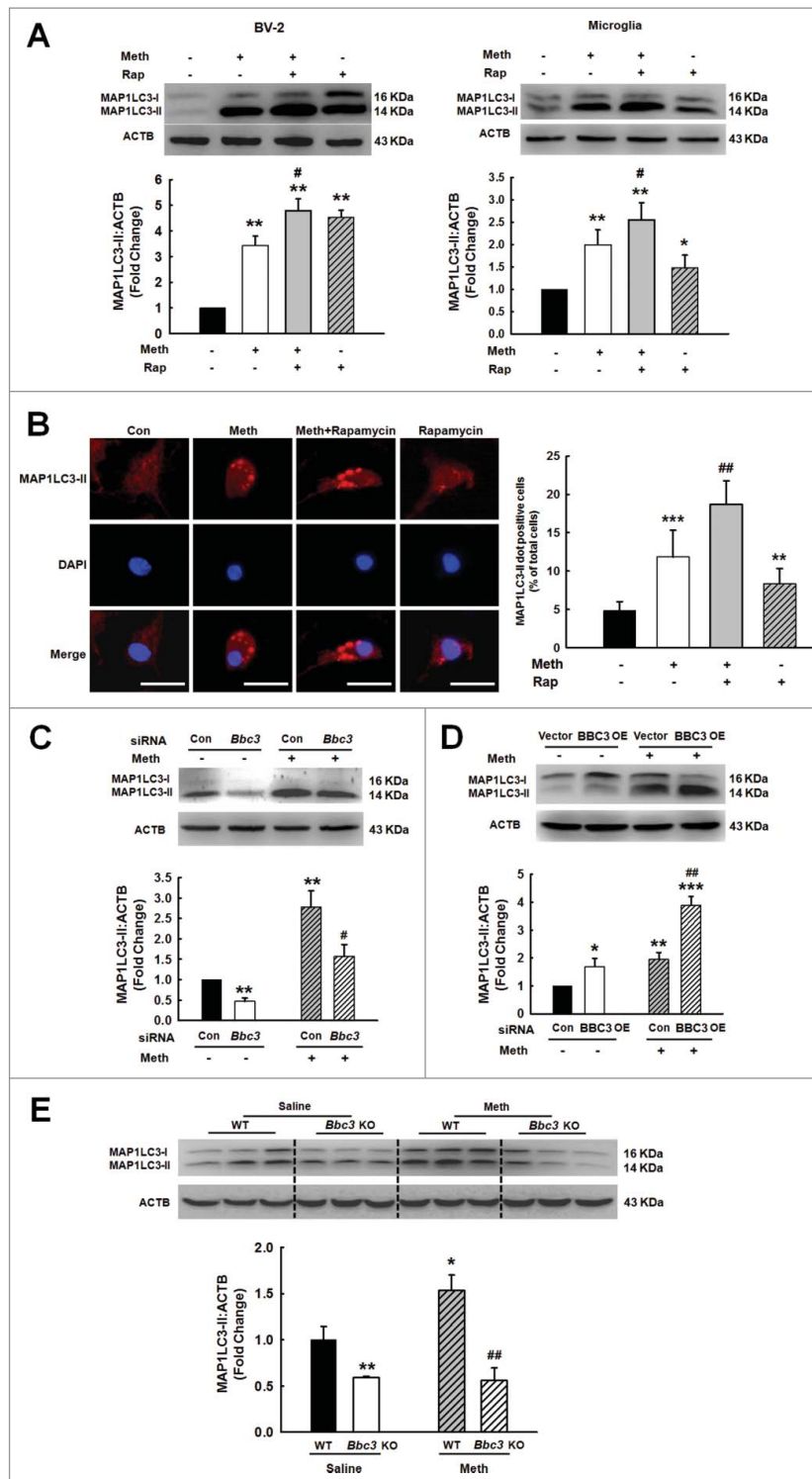


Figure 8. Role of BBC3 in methamphetamine-induced autophagy of microglia. (A) Pretreatment of BV-2 cells (left panel) and primary mouse microglia (right panel) with the autophagy inducer rapamycin (0.1 μ M) for 1 h enhanced the methamphetamine-induced increase in MAP1LC3-II expression. (B) Effect of methamphetamine on the formation of MAP1LC3-II puncta. Cells were pretreated with rapamycin for 1 h and then treated with methamphetamine (1.5 mM) for another 24 h. MAP1LC3-II puncta were then analyzed by confocal microscopy. Scale bar: 20 μ m. (C) Knockdown of *Bbc3* expression by siRNA decreased the methamphetamine-induced expression of MAP1LC3-II in primary mouse microglia. Primary mouse microglia were transfected with *Bbc3* siRNA for 24 h followed by methamphetamine treatment (1.5 mM) for another 24 h, and the cells were processed for detection of MAP1LC3-II expression using western blotting. (D) Transduction of primary mouse microglia with BBC3 OE lentivirus further enhanced the methamphetamine-induced increase in MAP1LC3-II expression in primary mouse microglia. Primary mouse microglia were transfected with BBC3 OE lentivirus for 24 h followed by methamphetamine treatment (1.5 mM) for another 24 h, and the cells were processed for detection of MAP1LC3-II expression using western blotting. All data are presented as the mean \pm SD of 3 independent experiments. *, $p < 0.05$, **, $p < 0.01$ and ***, $p < 0.001$ vs. the control group; #, $p < 0.05$ and ##, $p < 0.01$ vs. the methamphetamine-treated group using one-way ANOVA followed by the Holm-Sidak test. (E) Expression of MAP1LC3-II in the hippocampus of WT and *Bbc3* KO mice as determined by western blotting. WT and *Bbc3* KO mice were treated with methamphetamine (intraperitoneal, 30 mg/kg) for 48 h, followed by examination for autophagy. N = 6 animals/group. *, $p < 0.05$ and **, $p < 0.01$ vs. the saline-treated WT group; ##, $p < 0.01$ vs. the methamphetamine-treated WT group using one-way ANOVA followed by the Holm-Sidak test. Meth, methamphetamine; Rap, rapamycin.

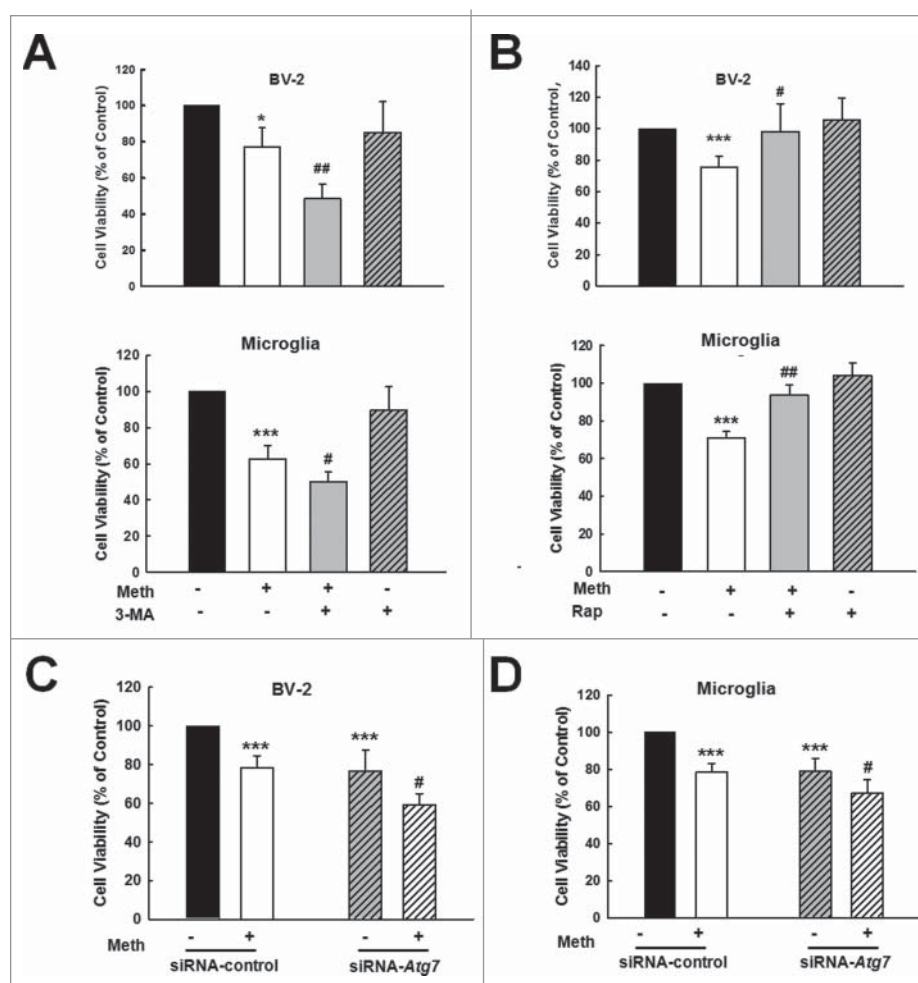


Figure 9. Role of autophagy in methamphetamine-induced microglial survival. (A) Pretreatment of cells with 3-MA augmented the methamphetamine-induced decrease in cell viability in BV-2 cells (upper panel) and in primary mouse microglia (lower panel). Cells were pretreated with 3-MA (1 mM) for 1 h and then treated with methamphetamine (1.5 mM) for 24 h. (B) Pretreatment of cells with the autophagy inducer rapamycin attenuated the methamphetamine-induced decrease in cell viability in BV-2 cells (upper panel) and in primary mouse microglia (lower panel). Cells were pretreated with rapamycin (0.1 μ M) for 1 h followed by methamphetamine (1.5 mM) treatment for 6 h. (C and D) Transfection of cells with *Atg7* siRNA lentivirus decreased cell viability in both BV-2 cells (C) and primary mouse microglia (D) as determined by CCK8 assay. Cells were transfected with *Atg7* siRNA lentivirus for 24 h and treated with methamphetamine (1.5 mM) for 24 h. All data are presented as the mean \pm SD of 3 independent experiments. *, $p < 0.05$ and ***, $p < 0.001$ vs. the control group; #, $p < 0.05$ and ##, $p < 0.01$ vs. the methamphetamine-treated group using one-way ANOVA followed by the Holm-Sidak test. Meth, methamphetamine; 3-MA, 3-methyladenine; Rap, rapamycin.

autophagy in methamphetamine-induced apoptosis, cells were treated with 3-MA, which enhanced the level of cleaved CASP3 in both BV-2 cells and primary mouse microglia (Fig. 10A and B). Conversely, pretreatment of cells with rapamycin significantly inhibited the increased level of cleaved CASP3 in both BV-2 cells and primary mouse microglia (Fig. 10C and D).

Role of *Mir143*-*BBC3* in methamphetamine-induced apoptosis and autophagy in vitro

Having determined that *Mir143* regulated *BBC3* expression, we next examined the role of *Mir143* in microglial survival. Primary mouse microglia were transduced with a lentivirus expressing *anti-Mir143*, and cell viability was assessed. As shown in Fig. 11A, transduction of cells with *anti-Mir143* lentivirus significantly inhibited the methamphetamine-induced decrease in cell survival as determined by CCK8 assay. The role of *Mir143* in methamphetamine-induced apoptosis and autophagy in microglia was further examined. Transduction of

cells with *anti-Mir143* lentivirus significantly enhanced the levels of cleaved CASP3 (Fig. 11B) and MAP1LC3-II (Fig. 11C) in primary mouse microglia. Next, to determine whether *anti-Mir143*-mediated functional effects depend specifically on the upregulation of *BBC3*, primary mouse microglia were cotransduced with lentiviral vectors expressing *anti-Mir143* and *Bbc3* siRNA. Transduction of cells with *anti-Mir143* lentivirus enhanced cell viability, and this effect was significantly inhibited in cells cotransduced with lentiviral vectors expressing *anti-Mir143* and *Bbc3* siRNA (Fig. 11D). Moreover, the transduction of cells with *anti-Mir143* lentivirus resulted in enhanced cleaved CASP3 and MAP1LC3-II (Figs. 11E and F), and this effect was inhibited in cells cotransduced with lentiviral vectors expressing *anti-Mir143* and *Bbc3* siRNA (Figs. 11E and F).

Reciprocally, transduction of cells with the *Mir143* precursor had opposing effects. To further determine whether *Mir143*-mediated functional effects depend specifically on *BBC3* suppression, an expression construct encoding the entire *BBC3*

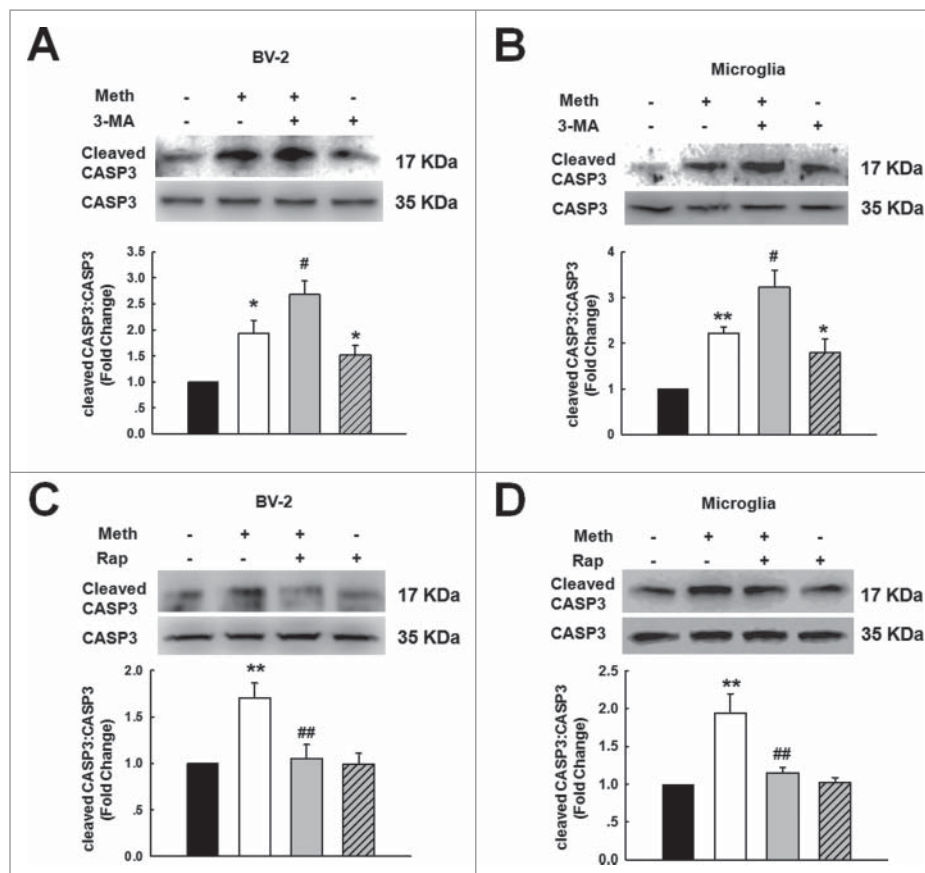


Figure 10. Role of autophagy in methamphetamine-induced microglial apoptosis. (A and B) Pretreatment with 3-MA (1 mM) for 1 h enhanced the level of cleaved CASP3 in both BV-2 cells (A) and primary mouse microglia (B). Cells were pretreated with 3-MA (1 mM) for 1 h followed by methamphetamine (1.5 mM) treatment for 6 h. (C and D) Pretreatment with rapamycin (0.1 μ M) for 1 h significantly decreased the level of cleaved CASP3 in both BV-2 cells (C) and primary mouse microglia (D). All data are presented as the mean \pm SD of 3 independent experiments. *, $p < 0.05$, and **, $p < 0.01$ vs. the control group; #, $p < 0.05$ and ##, $p < 0.01$ vs. the methamphetamine-treated group using one-way ANOVA followed by the Holm-Sidak test. Meth, methamphetamine; 3-MA, 3-methyladenine; Rap, rapamycin.

coding sequence but lacking the 3'-UTR (BBC3 OE), which yields an mRNA resistant to *Mir143*-mediated suppression, was generated. The transduction of cells with *Mir143* lentivirus decreased cell survival, and this effect was ameliorated in cells cotransduced with BBC3 OE lentivirus in primary mouse microglia (Fig. S11).

Role of *Mir143* in methamphetamine-induced microglial death in vivo

Our findings demonstrate that *Mir143*, which is involved in the regulation of BBC3 expression, plays a critical role in microglial apoptosis and autophagy. Notably, one of the unavoidable caveats of *in vitro* studies involving either BV-2 or primary microglia is their inherent ability to become activated during culture. Therefore, we sought to validate the role of *Mir143* in vivo by microinjecting *anti-Mir143* lentivirus into the hippocampus of C57BL/6J mice. C57BL/6J mice were microinjected bilaterally with either the *anti-Mir control*-RFP lentivirus or the *anti-Mir143*-RFP lentivirus in the hippocampus and monitored for microglial survival in response to methamphetamine. However, first determining the efficacy of *anti-Mir143*-RFP lentivirus transduction in vivo was important. As shown in Fig. 12A, RFP expression was largely restricted to the hippocampus, and a certain number of AIF1-positive cells colocalized with RFP. As expected, increased BBC3 expression was observed in the *anti-*

Mir143-injected side compared with that in the side injected with *anti-Mir control* (Fig. 12B). Two wk following lentivirus injections, the mice were administered methamphetamine (30 mg/kg), and AIF1-positive cells in the hippocampus were assessed. As shown in Fig. 12C and D, compared with the saline control group, *anti-Mir control*-RFP lentivirus-microinjected mice exhibited a decreased number of AIF1-positive microglia in the presence of methamphetamine, which was significantly attenuated by microinjection of *anti-Mir143*.

To further confirm the role of *Mir143* in methamphetamine-induced decrease in microglial survival, we sought to generate *mir143*^{-/-} mice. Because we failed to generate homozygous *mir143*^{-/-} mice from 8 littermates thus far, we used heterozygous *Mir143*^{+/-} mice to confirm our findings. As shown in Fig. 13A, *Mir143* expression was significantly decreased in heterozygous *Mir143*^{+/-} mice compared with WT mice. Moreover, methamphetamine treatment increased *Mir143* expression in the hippocampus of WT mice but not in *Mir143*^{+/-} mice (Fig. 13B). Consistent with the *in vitro* findings, methamphetamine treatment increased the mRNA level of *Bbc3* (Fig. S12A) but decreased BBC3 expression at the protein level (Fig. S12B) in the WT mice, which further confirming that the decreased expression of BBC3 was regulated at the post-transcriptional level in vivo. However, methamphetamine treatment failed to affect the expression of BBC3 at either the mRNA or protein level in *Mir143*^{+/-} mice compared with the

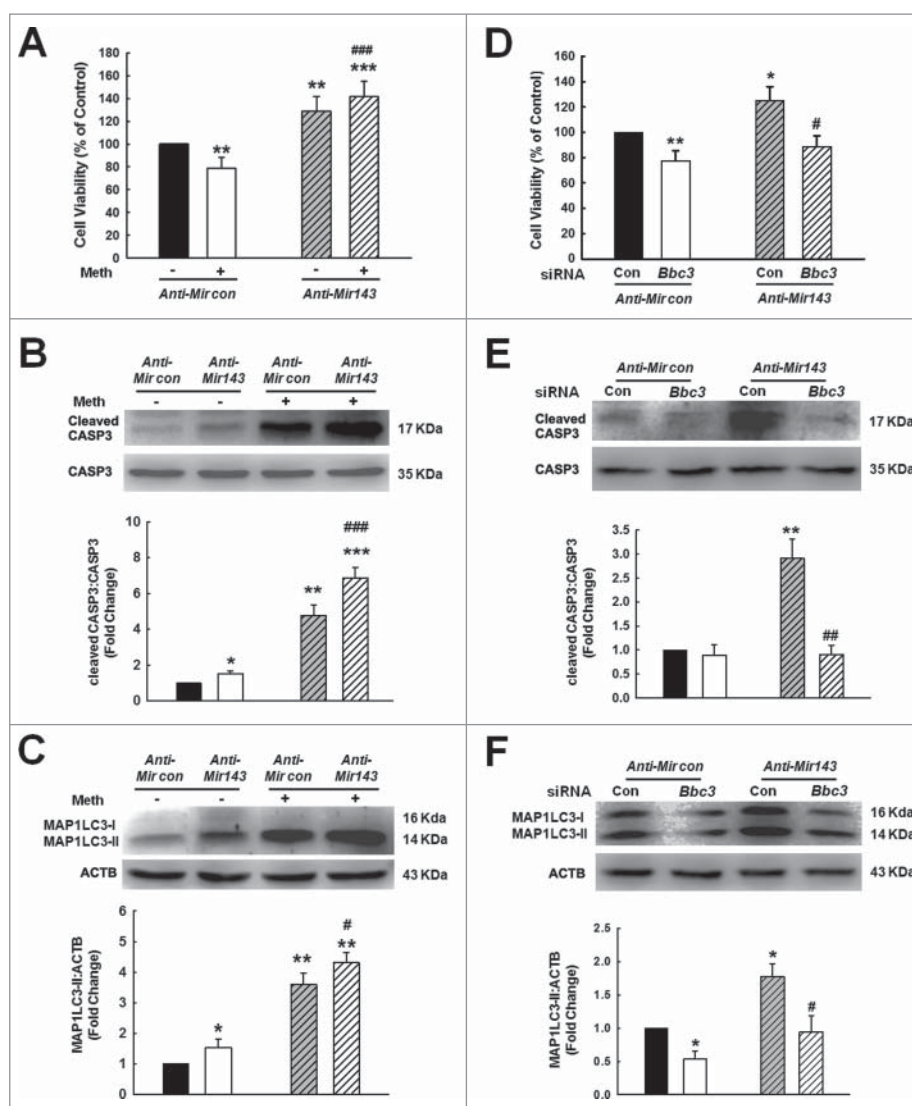


Figure 11. Role of *Mir143*-BBC3 in methamphetamine-induced apoptosis and autophagy in vitro. (A to C) Transduction of cells with *anti-Mir143* attenuated the methamphetamine-induced decrease in cell viability as determined by CCK8 assay (A) and enhanced the level of cleaved CASP3 (B) and MAP1LC3-II (C) as determined by western blotting. Cells were transduced with *anti-Mir143* lentivirus for 24 h and then treated with methamphetamine (1.5 mM) for 24 h to examine the cell viability and MAP1LC3-II expression and for 6 h to evaluate the level of cleaved CASP3. All data are presented as the mean \pm SD of 3 independent experiments. *, $p < 0.05$, **, $p < 0.01$ and ***, $p < 0.001$ vs. the *anti-Mircontrol* group; #, $p < 0.05$ and ###, $p < 0.001$ vs. the *anti-Mircontrol* treated with methamphetamine group using one-way ANOVA followed by the Holm-Sidak test. (D to F) Transduction of cells with the *Bbc3* siRNA lentivirus significantly inhibited the *anti-Mir143*-induced increase in cell viability as determined by CCK8 assay (D) and decreased the levels of cleaved CASP3 (E) and MAP1LC3-II (F) as determined by western blotting. Cells were transduced with *Bbc3* siRNA lentivirus for 24 h, and then were treated with methamphetamine (1.5 mM) for another 24 h to examine the cell viability and MAP1LC3-II expression, and for another 6 h to evaluate the level of cleaved CASP3. All data are presented as the mean \pm SD of 3 independent experiments. *, $p < 0.05$ and **, $p < 0.01$ vs. the *anti-Mircontrol* group; #, $p < 0.05$ and ##, $p < 0.01$ vs. the *anti-Mir143* cotransduced with siRNA-control group using one-way ANOVA followed by the Holm-Sidak test. Meth: methamphetamine.

saline control group (Fig. S12). To confirm the role of *Mir143* in methamphetamine-induced microglial survival, we examined microglial survival in *Mir143*^{+/-} mice. As shown in Fig. 13C and D, methamphetamine administration significantly decreased the number of AIF1-positive cells in the hippocampus of WT mice; however, methamphetamine failed to induce microglial death in *Mir143*^{+/-} mice. These findings thus underpin the role of *Mir143* in regulating the methamphetamine-mediated decrease in microglial survival in vivo.

Discussion

Our study provides new insights into the role of *Mir143* in the regulation of microglial survival: *Mir143* modulates BBC3 expression, which regulates the interplay of apoptosis and

autophagy. The modulation of *Mir143*-BBC3 expression may be a therapeutic intervention for the regulation of microglial survival in the context of drug abuse.

Our finding indicated that methamphetamine increased BBC3 expression with a concomitant increase in apoptosis, thus resulting in decreased cell viability. We anticipated that BBC3 deficiency would attenuate the methamphetamine-induced decrease in microglia survival. However, to our surprise, BBC3 deficiency failed to attenuate the methamphetamine-induced decrease in microglial survival and even exacerbated the decreased cell viability, contradicting the common view that BBC3 is an essential apoptosis inducer.^{14,15} This finding, along with the previous report that the number of microglia in the retina was significantly decreased in *Bbc3* KO mice compared with WT,⁴³ suggests a novel function of BBC3 in microglial survival.

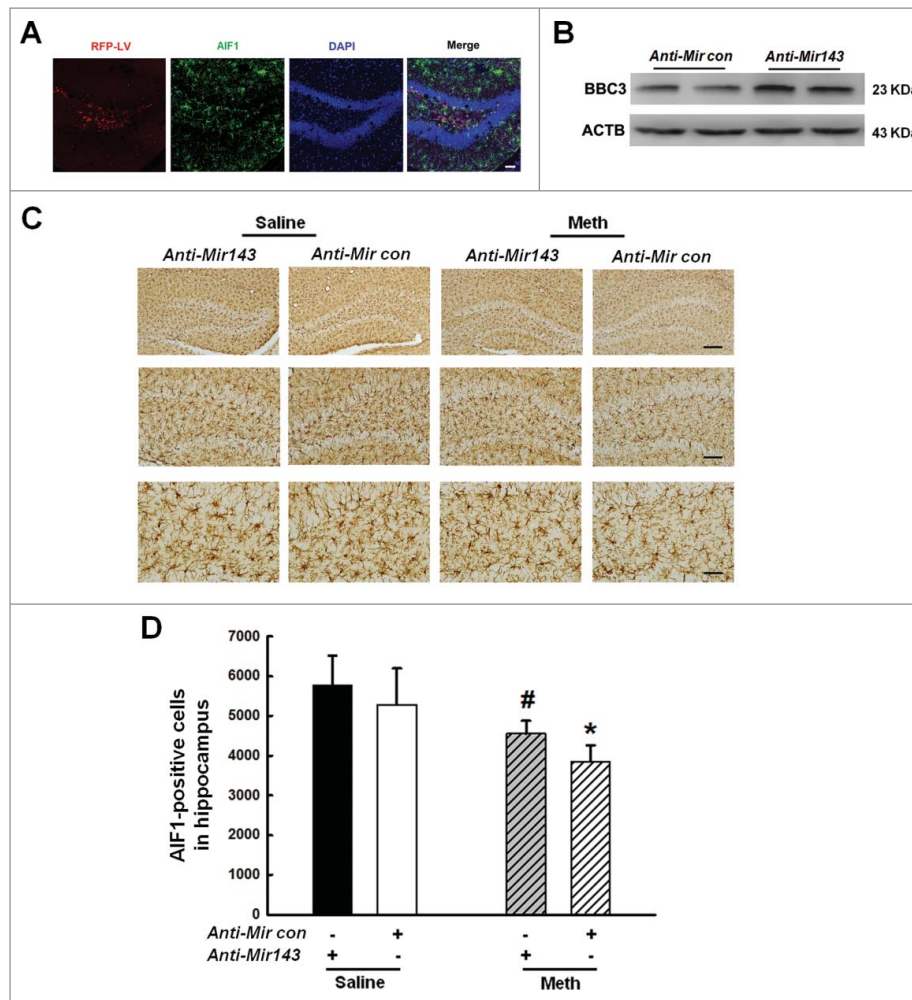


Figure 12. Role of *Mir143* in methamphetamine-induced microglial death in vivo. (A) Representative images of C57BL/6J mice microinjected with either *anti-Mir control*-RFP lentivirus or *anti-Mir143*-RFP lentivirus (LV) in microglia of the hippocampus. Scale bar: 100 μm . Mice were microinjected bilaterally with *anti-Mir*-RFP lentivirus ($2 \mu\text{l}$ of 10^9 viral genomes μl^{-1}) into the hippocampus, and 2 wk after microinjection, mice were sacrificed and examined for RFP and AIF1 expression. (B) *Anti-Mir143* lentivirus injection successfully increased BBC3 expression as determined by western blotting. Two wk after microinjection, mice were sacrificed and examined for BBC3 expression. (C) Effect of methamphetamine on the survival of microglia in the hippocampus of C57BL/6J mice, which were microinjected with either *anti-Mir control*-RFP lentivirus or *anti-Mir143*-RFP lentivirus. Two wk after microinjection, mice were treated with methamphetamine (intraperitoneal, 30 mg/kg) for another 48 h, followed by AIF1 immunostaining. Representative images of AIF1 immunostaining in the hippocampus of mice injected with saline or methamphetamine. Scale bars: 200 μm (upper panel), 100 μm (middle panel), and 50 μm (lower panel). (D) Stereology of AIF1-positive microglia in the hippocampus. $N = 5$ animals/group. *, $p < 0.05$ vs. the *anti-Mir control* mice treated with saline group; #, $p < 0.05$ vs. the *anti-Mir control* mice treated with methamphetamine-treated group using one-way ANOVA followed by the Holm-Sidak test. Meth, methamphetamine.

Mechanistically, our study indicated that the transcription factor TRP53 and *Mir143* co-coordinately regulated methamphetamine-induced BBC3 expression. This finding is in agreement with a previous study that demonstrated that *Mir9-5p* and SP1 coregulated target genes that cooperatively activate or block NF κ B target gene expression.⁴⁴ Consistent with previous studies showing that BBC3 is the downstream target of TRP53,^{16,45,46} our study also demonstrated that the TRP53 pathway was activated in methamphetamine-treated microglia and contributed to BBC3 expression. Indeed, methamphetamine induced an almost 2-fold increase in *Bbc3* mRNA levels. Intriguingly, western blot assay showed that methamphetamine treatment induced a transient increase in BBC3 protein levels followed by reduction to a level comparable to the control group, although the *Bbc3* mRNA level significantly increased simultaneously. This result strongly suggested that an additional mechanism negatively regulates BBC3 protein expression likely at the post-transcriptional level. Therefore, we further

examined the detailed mechanisms in this process and found that *Mir143* regulated BBC3 protein expression. Although mounting evidence has demonstrated the critical role of *Mir143* in cancer cells²⁴⁻²⁶ and in cell metabolism,²⁷ studies in microglia in the CNS are lacking. To our knowledge, our study is the first to indicate that *Mir143* regulates BBC3 expression, revealing a new mechanism for BBC3 expression.

Moreover, our study used comprehensive systems and approaches and demonstrated an unexpected function of BBC3, suggesting a functional property of BBC3 to exhibit apoptotic or autophagic activities under different conditions. A previous study indicated that current cancer therapies induce a tight interplay between autophagy and apoptosis.⁴⁷ Autophagy plays a dual role, either promoting cell survival or cell death in response to cancer treatments depending on the cellular context and on the nature of the treatments.⁴⁸ Consistent with these findings in cancer cells, methamphetamine increased BBC3 expression with concomitant increases in apoptosis and

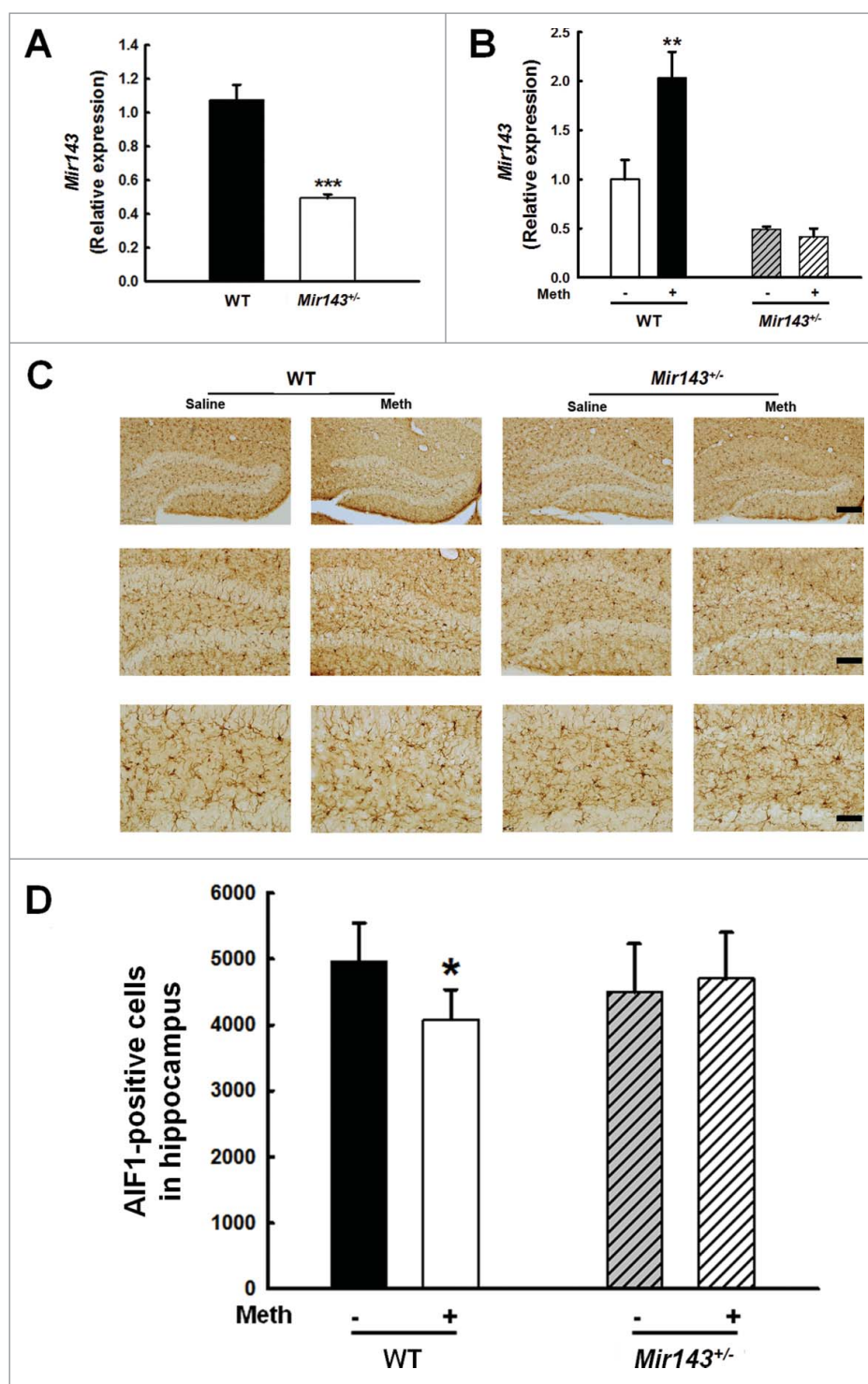


Figure 13. Role of *Mir143* in methamphetamine-induced decreased microglial survival in vivo. (A) *Mir143* expression was decreased in heterozygous *Mir143*^{+/-} mice compared with WT mice. WT and *Mir143*^{+/-} mice were treated with methamphetamine (intraperitoneal, 30 mg/kg) for 48 h. N = 6 animals/group. ***, $p < 0.001$ vs. the WT group using Student *t* test. (B) Administration of methamphetamine significantly increased hippocampal *Mir143* expression in WT mice but not in *Mir143*^{+/-} mice compared with the saline control group. WT and *Mir143*^{+/-} mice were treated with methamphetamine (intraperitoneal, 30 mg/kg) for 48 h. N = 6 animals/group. **, $p < 0.01$ vs. the saline-treated WT group using one-way ANOVA followed by the Holm-Sidak test. (C) Effect of methamphetamine on the survival of microglia in the hippocampus of heterozygous *Mir143*^{+/-} and WT mice. WT and *Mir143*^{+/-} mice were treated with methamphetamine (intraperitoneal, 30 mg/kg) for 48 h. Representative images of AIF1 immunostaining in the hippocampus of mice injected with saline or methamphetamine. Scale bars: 200 μ m (upper panel), 100 μ m (middle panel), and 50 μ m (lower panel). (D) Stereology of AIF1-positive microglia in the hippocampus. N = 5 animals/group. *, $p < 0.05$ vs. the saline-treated WT group using one-way ANOVA followed by the Holm-Sidak test. Meth, methamphetamine.

autophagy. The explanation for the consequent decrease in cell viability was because apoptosis overwhelmed autophagy, resulting in decreased cell viability in microglia treated with methamphetamine, as both apoptosis and autophagy cooperatively

regulated cell survival. However, why did BBC3 deficiency fail to reverse the decrease in cell viability induced by methamphetamine? A possible explanation for this observation could be that although BBC3 deficiency decreased methamphetamine-

induced apoptosis, it also decreased autophagy, as autophagy plays a prosurvival role in microglia (Fig. 5). Using both pharmacological and genetic approaches, we demonstrated that autophagy inhibition augmented the methamphetamine-induced decrease in cell viability, whereas the autophagy inducer rapamycin attenuated the methamphetamine-induced cell death. Our findings are consistent with that of a previous study that showed that methamphetamine induces autophagy as a prosurvival response in endothelial cells.⁴⁹ Our findings suggested that BBC3 exhibits an unexpected complex function in different contexts, acting as a survival and proliferative factor by modulating apoptosis and autophagy cooperatively. Because of its potent apoptotic activity, BBC3 has been commonly considered a promising therapeutic molecule for cancer treatment;¹⁵ however, the knockout or knockdown of BBC3 expression worsened the methamphetamine-induced decrease in microglial survival. Therefore, mechanisms of the observed pro-survival role of BBC3 could vary in different cellular environments, helping to advance our understanding of the intricate relationship between apoptosis and autophagy.

Lending credence to the role of *Mir143* in cell proliferation,^{24,26} our findings suggested that the transduction of primary microglia with *Mir143* decreased microglial survival. Intriguingly, *Mir143* further potentiated the methamphetamine-induced decrease in microglial viability. Reciprocally, inhibition of *Mir143* activity via *anti-Mir143* attenuated the decrease in cell viability in the presence of methamphetamine. Notably, *Bbc3* is not the only target gene of *Mir143*. Previous studies have indicated that *Mir143* exerts its tumor-suppressive function through targeting oncogenes such as SDC1, KRAS and CEBPA.^{24,25,50} Moreover, astrocyte-enriched *Mir29a* regulates BBC3 expression and reduces neuronal vulnerability to ischemia in the forebrain.⁵¹ Additionally, *Mir125b* exerts neuroprotection against ethanol-induced apoptosis by targeting *Bbc3*.⁵² To confirm whether BBC3 was involved in *anti-Mir143*-induced cell survival, we cotransduced microglia with lentiviral vectors expressing *anti-Mir143* and *Bbc3* siRNA. Intriguingly, the increased microglial survival induced by *anti-Mir143* was abrogated by cotransduction with *Bbc3* siRNA lentivirus. This finding was further confirmed by the cotransduction of cells with *Mir143* and BBC3 OE (lacking the 3'-UTR) as evidenced by the fact that *Mir143* failed to decrease cell survival in the presence of BBC3 OE lentivirus. These findings further underscore the role of the *Mir143*-BBC3 axis in mediating the methamphetamine-induced decrease in cell viability. Consistent with the role of the *Mir143*-BBC3 cascade in the survival of microglia, *Mir143*-BBC3 coregulated apoptosis and autophagy. These findings not only support the notion that the interplay of apoptosis and autophagy is a common mechanism of microglial survival with different effects^{47,48} but also add a novel molecular link between apoptosis and autophagy in the context of drug abuse.

These findings were validated *in vivo*, where a genetic approach using *anti-Mir143* lentivirus was employed. Microinjection of *anti-Mir143* lentivirus into the hippocampus of mice followed by methamphetamine injection resulted in the restoration of microglial survival, thus validating the role of *Mir143* in the survival of microglia. Taken together, our findings implicate *Mir143* as a regulator of microglia survival via its suppression of the target gene *Bbc3*. In the context of neurotoxicity induced by methamphetamine, when *Mir143* expression is upregulated, treatment with

anti-Mir143 may have a beneficial effect by dampening the decreased survival of microglia. Indeed, we observed that microinjecting *anti-Mir143* into the hippocampus attenuated the methamphetamine-induced decrease in microglial survival. Although this finding was further confirmed in heterozygous *Mir143*^{+/-} mice, one of the caveats of our study is the fact that we failed to obtain homozygous *mir143*^{-/-} mice from 35 littermates by breeding heterozygous *Mir143*^{+/-} mice, whereas a previous study successfully generated homozygous *mir143*^{-/-} mice.⁵³ This discrepancy could be attributed to the different source of embryonic stem cells or the different strain of mice. The reason for this discrepancy regarding the homozygous *mir143*^{-/-} mice is currently under investigation.

In response to cellular damage due to methamphetamine, the host is also capable of generating BBC3, which exerts somewhat paradoxically diverse roles as an inducer of both apoptosis and autophagy. Thus, depending on the specific context, the same host factor can manifest diverse activation responses that lead to diverse outcomes. The ultimate outcome of methamphetamine in the CNS is thus a result of the ensuing shift in balance between apoptosis and autophagy manifested over time following methamphetamine treatment. Here, we reported the diverse function of BBC3 as an inducer of both apoptosis and autophagy in the setting of methamphetamine abuse. Because this paradoxical regulation is a common theme of this type of factor, caution has to be exercised in the development of therapeutic targets involving these mediators.

In summary, *Mir143* plays a crucial role in microglial survival via the suppression of BBC3 expression and the subsequent cooperation of apoptosis and autophagy. Thus, the *Mir143*-BBC3 axis mediates a regulatory pathway that is critical for regulating microglial survival.

Methods

Reagents

Lentiviral vectors carrying *Mir143* OE (HB-LP140MI143), *anti-Mir143* (HB-LP240MA143), mouse *Bbc3* siRNA (HB-LP140240) and *Atg7* siRNA (HB-LP400si717) and adenoviral vector carrying mRFP-GFP-MAP1LC3 (HB-AP2100001) were purchased from HANBIO. BBC3 OE plasmid (pHA-BBC3; 16588 deposited by Bert Vogelstein) was obtained from Addgene. According to the sequence of *Bbc3*, the BBC3 OE lentivirus was packaged by HANBIO. Methamphetamine was ordered from the National Institute for the Control of Pharmaceutical and Biological Products. Control siRNA (sc-37007), mouse *Trp53* siRNA (sc-29436), mouse *Bbc3* siRNA (sc-37154), mouse *Becn1* siRNA (sc-29798) and pifithrin- α hydrobromide (sc-45050) were obtained from Santa Cruz Biotechnology. Rapamycin (R0395) and 3-methyladenine (M9281) were purchased from Sigma-Aldrich.

Animals

Mir143 mutant mice (Mutant Mouse Resource & Research Centers supported by NIH; https://www.mmrrc.org/catalog/cellLineSDS.php?mmrrc_id=43338) were generated using a standard mirKO targeting vector containing a PGK-EM7 promoter puroDtk selection cassette flanked by recombinase sites as

described in a previous study.⁵⁴ These mice were obtained from a model animal resource information platform (<http://www.nbri-nju.com/strain-view-T000498?search=mi&descriptor=true&page=3>). Genotyping of mice or embryos was routinely performed with tail specimens or embryonic tissue by PCR using a mixture of 2 primers. The primer sequences used were as follows: *Mir143-3p* common forward, 5'-TCTA-GAAAGTATAGGAACTTCCATGGTC-3' (p1), and *Mir143-3' gsp* reverse-1, 5'-CCCAGAATGGGTAGATGTAGCGTCTT-3' (p2); *Mir143-5' gsp* forward, 5'-TGGGTTCCATCTTTAGCACTGAAA-3' (p3), and *Mir143-5' common* reverse, 5'-ATAGCATAACATTATACGAAGTTATCACTGG-3' (p4). The PCR with p1-p2 primers yields a 272-base pair (bp) product and the PCR with p3-p4 primers yields 220-bp products for heterozygous mice and negative bands for WT mice. The PCR with p3-p2 primers yields 3163-bp and 565-bp products for heterozygous and WT mice, respectively. Heterozygous animals were used to obtain homozygous *mir143*^{-/-} mice. Unfortunately, we failed to generate homozygous *mir143*^{-/-} mice from 35 littermates thus far; therefore, heterozygous mice were used in our current study. However, a previous study successfully generated *mir143* mutant mice using a different source of embryonic stem cells.⁵³

Bbc3 KO mice were kindly shared by Dr. Gerard Zambetti at St. Jude Children's Research Hospital, Inc., and by Dr. Tao Cheng from State Key Laboratory of Experimental Hematology, Institute of Hematology and Blood Disease Hospital, Chinese Academy of Medical Sciences and Peking Union Medical College. C57BL/6J mice (male, 6-8 wk) were purchased from the Comparative Medicine Center, Yangzhou University (Yangzhou, China). All animals were housed under conditions of constant temperature and humidity on a 12h light: 12h dark cycle, with lights on at 07:00 a.m. Food and water were available *ad libitum*. Animals were deeply anesthetized by an overdose of isoflurane followed by pneumothorax before perfusion. All animal procedures were performed according to the protocols approved by the Institutional Animal Care and Use Committee of the Medical School, Southeast University.

Cell cultures

Primary mouse microglia cells were obtained from postnatal (P1 to P2) C57BL/6J mice, which were purchased from the Comparative Medicine Center, Yangzhou University. After the membranes and large blood vessels were dissociated, the dissected brain cortices in phosphate-buffered saline (PBS; 137 mM NaCl, 2.7 mM KCl, 10 mM Na₂HPO₄, 2 mM KH₂PO₄) supplemented with brain tissues were digested by trypsin-EDTA (Gibco, 25200056). Cells were seeded in 25-cm² cell culture flasks pre-coated with poly-D-lysine (Sigma-Aldrich, P0296) with Dulbecco's modified Eagle's medium (DMEM) supplemented with fetal bovine serum (10% v/v) and penicillin-streptomycin (1% v/v). After 3 d, the medium was changed for the first time. Seven days later, the medium was replaced every 3 d, and CSF2/GM-CSF (colony stimulating factor 2 [granulocyte-macrophage]; 0.25 ng/ml; PeproTech, 315-03) was added to the flasks to promote microglial proliferation. The microglia were detached from the flasks by shaking and

collected from the cell medium by centrifugation at 1500×g for 5 min.

BV-2 cells are a murine immortalized microglial cell line. These cells were used to characterize the effects of methamphetamine on brain microglia. BV-2 cells were obtained from the China Center for Type Culture Collection, routinely maintained in DMEM (10% fetal bovine serum, 1% penicillin-streptomycin) and incubated in 5% CO₂ at 37°C.

Luciferase activity assays

The 990-bp human *BBC3* gene 3'-UTR containing the putative *Mir143* target site was PCR-amplified from human genomic DNA using forward (5'-GCGGCTCGAGAGCCCAATTA GGTGCCTG-3') and reverse (5'-AATGCGGCCG CCCACTGTTCCAATCTGATTTTAT-3') primers, and the DNA fragment was cloned into the XhoI and NotI sites on the 3' end of the *luc2* gene in the pmiR-RB-REPORTTM vector (RiboBio, UR100000). For the pmiR-RB-*Bbc3* 3'-UTR-*Mir143*-target-mutant vector, the *Mir143* target site (CATCTCA) within the *BBC3* 3'-UTR was changed to GTAGAGT by PCR mutagenesis with primers *Bbc3-Mir143T-F* (5'-CCCACCACGTAGAGTG-GAAAGGCTGTTGTGCTG-3') and *Bbc3-Mir143T-R* (5'-GCCTTTCCACTCTACGTGGTGGGCGGCAGAGGC-3'). Briefly, 293T cells were transfected with *Mir143* OE pLV-[*hsa-Mir143*] vector and the target plasmid pmiR-RB-*Bbc3*-3'-UTR or pmiR-RB-*Bbc3*-3'-UTR-*Mir143*-target-mutant in a molar ratio of 50:1. The *Mir control* pLV-[*Mir control*] plasmid was used as a negative control. Luciferase activity was determined 24 h post-transfection, and the reporter assay was performed following the manufacturer's protocol (Promega, E2920). *Renilla* luciferase activity was normalized to firefly luciferase activity and expressed as a percentage of the control (n > 3, performed in 5 wells each time).

Western blot analysis

Proteins were extracted in RIPA lysis buffer (Beyotime, P0013B). The nuclear protein fraction was extracted using a KeyGen Nuclear and Cytoplasmic Protein Extraction Kit (Key-GenBiotech, KGP150). For cytosolic and mitochondrial protein extraction, a Cell Mitochondria Isolation Kit (Beyotime, C3601) was used according to the manufacturer's instructions. Proteins were separated by sodium dodecyl sulfate-polyacrylamide gel electrophoresis (12%) and electrophoretically transferred onto polyvinylidene fluoride membranes. The membranes were blocked with 5% nonfat dry milk in Tris-buffered saline (50 mM Tris, 150 mM NaCl, pH 7.6) with Tween-20 (0.05%; Beyotime, ST825), probed with antibodies overnight at 4°C, and then incubated with horseradish peroxidase-conjugated goat anti-mouse/rabbit IgG secondary antibody (1:2000). The antibodies used were as follows: anti-MAP1LC3 (L7543) from Sigma-Aldrich; anti-BAX (2772), anti-BCL2L1 (2764), anti-cleaved CASP9 (9509), anti-CASP9 (9504), anti-cleaved CASP3 (9664), anti-CASP3 (9662), anti-H3F3/Histone H3 (9715), anti-ATG7 (2631), anti-phosphorylated (p)-AKT1 (9271), anti-AKT1 (9272), anti-p-MTOR (2971), anti-MTOR (2983), anti-p-RPS6KB1(9206), anti-p-EIF4EBP1 (9455), anti-EIF4EBP1 (9644), anti-p-RPS6 (2211), anti-p-MAPK1 (9101),

and anti-MAPK1 (9107) from Cell Signaling Technology; anti-BBC3 (sc-28226), anti-TRP53 (FL-393), anti-GAPDH (sc-32233), and anti-BECN1 (sc-4834) from Santa Cruz Biotechnology; anti-SQSTM1 (18420), anti-BCL2 (12789), anti-CYCS (10993), and anti-COX4I1/COXIV (11242) from Proteintech; anti-NOS2 (ab3523) from Abcam and anti-ACTB/ β -actin (BS6007M) from Bioworld. Detection was performed using a MicroChem4.2[®] (DNR, Israel) digital image scanner. Band intensity was quantified by ImageJ software (NIH).

Real-time PCR

Total RNA isolated from cells was subjected to reverse transcription using a PrimeScript RT Master Mix Kit (TaKaRa, RR036). Real-time PCR analysis was performed for *Bbc3* (forward primer: 5'-ACGACCTCAACGCGCAGTA-3'; reverse primer: 5'-CTAGTTGGGCTCCATTTCTGG-3') and *Actb* (forward primer: 5'-CTAGCACCATGAAGATCAAGAT-3'; reverse primer: 5'-CCAGGATAGAGCCAC CAA-3'). Relative quantification was performed using TaKaRa SYBR[®] Premix TaqTM (TbIRNase H Plus; TaKaRa, RR420). Specific primers and probes for mature *Mir143* and *Rnu6* snRNA were obtained from RiboBio. All reactions were run in triplicate. The amount of *Mir143* was obtained by normalizing to *Rnu6* snRNA relative to the control as previously reported.⁵⁵

Fluorescence in situ hybridization combined with immunostaining

Treated primary mouse microglia were fixed in 4% paraformaldehyde for 15 min and incubated in PBS overnight at 4°C. Cells were permeabilized with 0.3% Triton X-100 (Biosharp, BS363A) in PBS for 15 min, pre-hybridized in hybridization buffer (50% formamide, 10 mM Tris-HCl, pH 8.0, 200 μ g/ml yeast tRNA [Invitrogen, 15401-029], 1X Denhardt's solution [Sigma-Aldrich, D2532], 600 mM NaCl, 0.25% SDS [Invitrogen, #15553-027], 1 mM EDTA, 10% dextran sulfate [Sigma-Aldrich, 8906-100]) for 1 h at 37°C. Then, the slides were heated to 65°C for 5 min in hybridization buffer with 2 nM commercially available digoxigenin-labeled *Mir143* probe (Exiqon, 38515-15) followed by hybridization at 37°C overnight. The next day, the slides were washed 3 times in 2X SSC (3 M NaCl, 0.3 M sodium citrate, pH 7.4) and twice in 0.2X SSC at 42°C. The slides were then blocked with 1% BSA (Biosharp, BS043D) and 3% normal goat serum (ZSGB-BIO, ZLI-9056) in PBS for 1 h at room temperature and incubated with horseradish peroxidase-conjugated anti-digoxigenin antibody (Roche Diagnostics GmbH, 11207733910) overnight at 4°C. After the slides were washed 3 times with TBS, they were incubated with a TSA Cy5 kit (PerkinElmer, NEL745001KT) for 10 min at room temperature. The samples were washed once with 0.1% Tween-20 in PBS, twice in PBS and once in DEPC water (Sigma-Aldrich, V900882-10ML); blocked with 1% BSA and 3% normal goat serum in 1X PBS for 1 h at room temperature; and incubated with anti-AIF1 antibody (Wako, 019-19741) overnight at 4°C. The slides were washed twice with PBS and incubated with Alexa Fluor 488-conjugated goat anti-rabbit IgG (Invitrogen, A11008) antibody for 1 h at room temperature. Then, the slides were washed twice with PBS and mounted

with Prolong gold anti-fade reagent containing DAPI (SouthernBiotech, 0100-20). The specificity of the *Mir143* signal in FISH experiments was confirmed by comparison with a scrambled control. Unlike the *Mir143* probe, the scramble probe showed no signal in microglia.

Microinjection of anti-Mir143

Eight-wk-old C57BL/6J mice were microinjected bilaterally with either *anti-Mir control*-RFP lentivirus or the *anti-Mir143*-RFP lentivirus (2 μ l of 10⁹ viral genomes μ l⁻¹, HANBIO, HB-LP240MA143) into the hippocampus using the following microinjection coordinates: 2.06 mm behind the bregma, \pm 1.5 mm lateral from the sagittal midline, at the depth of 1.7 mm to skull surface. To evaluate the effect of *anti-Mir143* on the methamphetamine-induced decrease in microglial survival, 2 wk after microinjection of lentivirus, 8 mice were divided into 2 groups (N = 5; male). One group was treated with saline, and the other group was treated with methamphetamine (intraperitoneal, 30 mg/kg). The methamphetamine was injected every 2 h for a total of 4 times/day. Two d later, these animals were perfused and sectioned followed by AIF1 staining to assess microglial activation.

Immunostaining and image analysis

According our previous study,⁵⁶ the sections encompassing the entire hippocampus were cut into 35 μ m sections on a cryostat. The sections were incubated with H₂O₂ for 10 min, permeabilized with 0.3% Triton X-100 in PBS for 15 min and blocked with 10% normal goat serum in 0.3% Triton X-100 for 1 h at room temperature. The sections were then incubated with rabbit anti-AIF1 antibody (Wako, 019-19741) overnight at 4°C. The next day, the sections were washed, incubated with biotinylated goat anti-rabbit IgG (Vector Laboratories, BA-1000) in PBS for 1 h at room temperature, and then incubated with VECTASTAIN[®] (VECTASTAIN[®] ABC Kit, Vector Laboratories, PK-6200) for 1 h. The horseradish peroxidase reaction product was visualized using an enhanced DAB peroxidase substrate kit (Vector Laboratories, SK-4100). The immunostaining signals were quantitatively analyzed using the optical Fractionator method with Microbrightfield Stereo-Investigator software (Stereo Investigator software, Microbrightfield, VT, USA). The total number of AIF1 microglia in the entire area of the hippocampus was counted from 4 or 5 samples per group.

MTT assay

Cell viability was measured by MTT assay. Cells were seeded in 96-well plates for 2 d and treated with different concentrations of methamphetamine for 24 h. MTT dye (20 μ l, 5 mg/ml; Biosharp, BS030C) was added to each well, and the cells were then incubated in a CO₂ incubator at 37°C for 1.5 h. The medium was aspirated from each well, and DMSO (200 μ l) was added to dissolve the formazan crystals. The absorbance of each well was obtained using a Synergy H1 Multi-Mode Reader (BioTek, Winooski, VT, USA) with a reference wavelength of 570 nm.

CCK8 assay

Cell viability was also measured using a CCK8 kit from Yeasen (40203ES80). Cells were plated at a density of 2×10^4 cells/well in a 96-well plate. After the cells were exposed to methamphetamine for 24 h, CCK-8 (10 μ l) was added to each well of the 96-well plate, and the plate was incubated for 1.5 h at 37°C. Viable cells were counted by absorbance measurements at 450 nm using a Synergy H1 Multi-Mode Reader (BioTek, Winooski, VT, USA).

Trypan blue exclusion assay

Cells were cultured in 24-well plates and treated with 1.5 mM methamphetamine. After 24 h, the cells were collected and then stained with trypan blue dye for 5 min at room temperature. Cells were counted by 4 independent hemocytometer counts. Cell death was determined as the percentage of dead cells over the total number of cells according to a previous study.⁵⁷

Measurement of the mitochondrial membrane potential

The integrity of the inner mitochondrial membrane was measured by observing the potential gradient across this membrane using a mitochondrial membrane potential assay kit with JC-1 (Beyotime, C2006). Cells were grown on cover slips or in 96-well plates and incubated with JC-1 dye at 37°C for 20 min. The cells were then washed twice with PBS. The cells on cover-slips or in 96-well plates were analyzed immediately using a confocal microscope (Olympus FV1000, Center Valley, PA, USA) or a Synergy H1 Multi-Mode Reader (BioTek, Winooski, VT, USA). Red emission indicates membrane potential-dependent JC-1 aggregates in mitochondria. Green fluorescence reflects the monomeric form of JC-1 appearing in the cytoplasm after mitochondrial membrane depolarization.

Transmission electron microscopy assay

Cells were cultured in 24-well plates and treated with 1.5 mM methamphetamine. After the cells were incubated with methamphetamine for 24 h, the treated cells were harvested in a 1.5 ml microcentrifuge tube for each sample. Cells were washed with cold PBS once and fixed in a mixture of 2% glutaraldehyde and 2% formaldehyde in 0.1 M sodium cacodylate buffer (pH 7.4) at 4°C overnight. All specimens were washed 4 times in 0.1 M sodium cacodylate buffer (pH 7.4) containing 264 mM sucrose (Sinopharm Chemical Reagent Co., Ltd, 10021418) before being transferred to 1% osmium tetroxide in 0.1 M sodium cacodylate (pH 7.4) for 2 h. The specimens were then washed 3 times in ddH₂O and stained in 2% aqueous uranyl acetate for 2 h. The specimens were dehydrated in an ethanol series, infiltrated in propylene oxide 2 times, and embedded in Epon812 (SPI Science, 02659-AB). Ultra-thin sections (90-nm thick) were cut using a Leica UC7 with a diamond knife. Grids were post-stained with 2% saturated uranyl acetate in 50% ethanol and 1% lead citrate (pH 12), examined using H-7650 electron microscope (Hitachi, Japan), and recorded with a Ganton830 digital camera.

Immunoprecipitation

To investigate the interaction between BECN1 with BCL2, cells were treated with 1.5 mM methamphetamine and lysed with RIPA buffer. In total, 100 μ l protein was incubated with 1 μ l BECN1 antibody overnight at 4°C and precipitated with 20 μ l Protein A/G PLUS-Agarose (Santa Cruz Biotechnology, sc-2003). After the cell pellets were rotated at 4°C for 90 min, the cell pellets were rinsed twice with 1 ml RIPA lysis buffer and boiled for 5 min with 5XSDS loading buffer (6 μ l) and RIPA lysis buffer (24 μ l). Then, the protein complexes were detected using BCL2 antibody; the input protein (without antibody addition) served as a control to confirm that equal amounts of total protein were used.

Statistical analyses

Statistical analysis was performed using Student *t* test or one-way analysis of variance (ANOVA) followed by the Holm-Sidak test (SigmaPlot 11.0). The appropriate tests are indicated in the figure legends. The results were considered significant if $p < 0.05$ by ANOVA.

Abbreviations

3-MA	3-methyladenine
ACTB	actin, beta
AICD	activation-induced cell death
AIF1	allograft inflammatory factor 1
AKT1	thymoma viral proto-oncogene 1
ATG7	autophagy-related 7
BafA1	bafilomycinA ₁
BAX	BCL2-associated X protein
BBC3	BCL2 binding component 3
BCL2	B-cell leukemia/lymphoma 2
BCL2L1	BCL2-like 1
BECN1	Beclin 1, autophagy related
BH3	BCL2-homology 3
CASP3	caspase 3
CASP9	caspase 9
CCK8	Cell Counting Kit-8
CNS	central nervous system
COX4I1	cytochrome c oxidase subunit IV isoform 1
CQ	chloroquine
CSF2/GM-CSF	colony stimulating factor 2 (granulocyte-macrophage)
CYCS	cytochrome c, somatic
DAPI	4',6-diamidino-2-phenylindole
DMEM	Dulbecco's modified Eagle's medium
EIF4EBP1	eukaryotic translation initiation factor 4E binding protein 1
FISH	fluorescence in situ hybridization
GAPDH	glyceraldehyde-3-phosphate dehydrogenase
H3F3	H3 histone, family 3
KO	knockout
MAP1LC3	microtubule-associated protein 1 light chain 3
MAPK1	mitogen-activated protein kinase 1
Meth	methamphetamine
Mir143	microRNA143

miRs	microRNAs
MTOR	mechanistic target of rapamycin (serine/threonine kinase)
NO	nitric oxide
NOS2	nitric oxide synthase 2, inducible
OE	overexpression
PCR	polymerase chain reaction
RPS6	ribosomal protein S6
RPS6KB1	ribosomal protein S6 kinase, polypeptide 1
SQSTM1	sequestosome 1
TRP53	transformation related protein 53
TUNEL	terminal deoxynucleotidyl transferase-mediated dUTP nick end-labeling
UTR	untranslated region
WT	wild type

Disclosure of potential conflicts of interest

No potential conflicts of interest were disclosed.

Funding

This work was supported by grants from the National Natural Science Foundation of China (No. 81322048 and No. 81473190). We were also awarded grants from the Jiangsu Specially Appointed Professor and the Major State Basic Research Development Program of China (973 Program) (2013CB733800, 2013CB733803) and the Postdoctoral Research Start Foundation of Southeast University (1124000342).

References

- [1] Schepers RJ, Oyler JM, Joseph RE, Jr., Cone EJ, Moolchan ET, Huestis MA. Methamphetamine and amphetamine pharmacokinetics in oral fluid and plasma after controlled oral methamphetamine administration to human volunteers. *Clin Chem* 2003; 49:121-32; PMID:12507968; <http://dx.doi.org/10.1373/49.1.121>
- [2] Kaushal N, Matsumoto RR. Role of sigma receptors in methamphetamine-induced neurotoxicity. *Curr Neuropharmacol* 2011; 9:54-7; PMID:21886562; <http://dx.doi.org/10.2174/157015911795016930>
- [3] Davalos D, Grutzendler J, Yang G, Kim JV, Zuo Y, Jung S, Littman DR, Dustin ML, Gan WB. ATP mediates rapid microglial response to local brain injury in vivo. *Nat Neurosci* 2005; 8:752-8; PMID:15895084; <http://dx.doi.org/10.1038/nn1472>
- [4] Nimmerjahn A, Kirchhoff F, Helmchen F. Resting microglial cells are highly dynamic surveillants of brain parenchyma in vivo. *Science* 2005; 308:1314-8; PMID:15831717; <http://dx.doi.org/10.1126/science.1110647>
- [5] Escubedo E, Guitart L, Sureda FX, Jimenez A, Pubill D, Pallas M, Camins A, Camarasa J. Microgliosis and down-regulation of adenosine transporter induced by methamphetamine in rats. *Brain Res* 1998; 814:120-6; PMID:9838075; [http://dx.doi.org/10.1016/S0006-8993\(98\)01065-8](http://dx.doi.org/10.1016/S0006-8993(98)01065-8)
- [6] Asanuma M, Tsuji T, Miyazaki I, Miyoshi K, Ogawa N. Methamphetamine-induced neurotoxicity in mouse brain is attenuated by ketoprofen, a non-steroidal anti-inflammatory drug. *Neurosci Lett* 2003; 352:13-6; PMID:14615038; <http://dx.doi.org/10.1016/j.neulet.2003.08.015>
- [7] LaVoie MJ, Card JP, Hastings TG. Microglial activation precedes dopamine terminal pathology in methamphetamine-induced neurotoxicity. *Exp Neurol* 2004; 187:47-57; PMID:15081587; <http://dx.doi.org/10.1016/j.expneurol.2004.01.010>
- [8] Thomas DM, Dowgiert J, Geddes TJ, Francescutti-Verbeem D, Liu X, Kuhn DM. Microglial activation is a pharmacologically specific marker for the neurotoxic amphetamines. *Neurosci Lett* 2004; 367:349-54; PMID:15337264; <http://dx.doi.org/10.1016/j.neulet.2004.06.065>
- [9] Thomas DM, Kuhn DM. Attenuated microglial activation mediates tolerance to the neurotoxic effects of methamphetamine. *J Neurochem* 2005; 92:790-7; PMID:15686480; <http://dx.doi.org/10.1111/j.1471-4159.2004.02906.x>
- [10] Sekine Y, Ouchi Y, Sugihara G, Takei N, Yoshikawa E, Nakamura K, Iwata Y, Tsuchiya KJ, Suda S, Suzuki K, et al. Methamphetamine causes microglial activation in the brains of human abusers. *J Neurosci* 2008; 28:5756-61; PMID:18509037; <http://dx.doi.org/10.1523/JNEUROSCI.1179-08.2008>
- [11] Yun HJ, Yoon JH, Lee JK, Noh KT, Yoon KW, Oh SP, Oh HJ, Chae JS, Hwang SG, Kim EH, et al. Daxx mediates activation-induced cell death in microglia by triggering MST1 signalling. *Embo J* 2011; 30:2465-76; PMID:21572393; <http://dx.doi.org/10.1038/emboj.2011.152>
- [12] Chipuk JE, Green DR. PUMA cooperates with direct activator proteins to promote mitochondrial outer membrane permeabilization and apoptosis. *Cell Cycle* 2009; 8:2692-6; PMID:19652530; <http://dx.doi.org/10.4161/cc.8.17.9412>
- [13] Thakur VS, Ruhul Amin AR, Paul RK, Gupta K, Hastak K, Agarwal MK, Jackson MW, Wald DN, Mukhtar H, Agarwal ML. p53-Dependent p21-mediated growth arrest pre-empts and protects HCT116 cells from PUMA-mediated apoptosis induced by EGCG. *Cancer Lett* 2010; 296:225-32; PMID:20444544; <http://dx.doi.org/10.1016/j.canlet.2010.04.012>
- [14] Yu J, Zhang L. PUMA, a potent killer with or without p53. *Oncogene* 2008; 27 Suppl 1: S71-83; PMID:19641508; <http://dx.doi.org/10.1038/onc.2009.45>
- [15] Yu J, Zhang L, Hwang PM, Kinzler KW, Vogelstein B. PUMA induces the rapid apoptosis of colorectal cancer cells. *Mol Cell* 2001; 7:673-82; PMID:11463391; [http://dx.doi.org/10.1016/S1097-2765\(01\)00213-1](http://dx.doi.org/10.1016/S1097-2765(01)00213-1)
- [16] Nakano K, Vousden KH. PUMA, a novel proapoptotic gene, is induced by p53. *Mol Cell* 2001; 7:683-94; PMID:11463392; [http://dx.doi.org/10.1016/S1097-2765\(01\)00214-3](http://dx.doi.org/10.1016/S1097-2765(01)00214-3)
- [17] O'Neill LA, Sheedy FJ, McCoy CE. MicroRNAs: the fine-tuners of Toll-like receptor signalling. *Nat Rev Immunol* 2011; 11:163-75; PMID:21331081; <http://dx.doi.org/10.1038/nri2957>
- [18] Johnnidis JB, Harris MH, Wheeler RT, Stehling-Sun S, Lam MH, Kirak O, Brummelkamp TR, Fleming MD, Camargo FD. Regulation of progenitor cell proliferation and granulocyte function by microRNA-223. *Nature* 2008; 451:1125-9; PMID:18278031; <http://dx.doi.org/10.1038/nature06607>
- [19] Ponomarev ED, Veremeyko T, Barteneva N, Krichevsky AM, Weiner HL. MicroRNA-124 promotes microglia quiescence and suppresses EAE by deactivating macrophages via the C/EBP-alpha-PU.1 pathway. *Nat Med* 2011; 17:64-70; PMID:21131957; <http://dx.doi.org/10.1038/nm.2266>
- [20] O'Connell RM, Rao DS, Chaudhuri AA, Baltimore D. Physiological and pathological roles for microRNAs in the immune system. *Nat Rev Immunol* 2010; 10:111-22; PMID:20098459; <http://dx.doi.org/10.1038/nri2708>
- [21] Bazzoni F, Rossato M, Fabbri M, Gaudiosi D, Mirolo M, Mori L, Tamassia N, Mantovani A, Cassatella MA, Locati M. Induction and regulatory function of miR-9 in human monocytes and neutrophils exposed to proinflammatory signals. *Proc Natl Acad Sci U S A* 2009; 106:5282-7; PMID:19289835; <http://dx.doi.org/10.1073/pnas.0810909106>
- [22] Cardoso AL, Guedes JR, Pereira de Almeida L, Pedrosa de Lima MC. miR-155 modulates microglia-mediated immune response by down-regulating SOCS-1 and promoting cytokine and nitric oxide production. *Immunology* 2012; 135:73-88; PMID:22043967; <http://dx.doi.org/10.1111/j.1365-2567.2011.03514.x>
- [23] Ponomarev ED, Veremeyko T, Weiner HL. MicroRNAs are universal regulators of differentiation, activation, and polarization of microglia and macrophages in normal and diseased CNS. *Glia* 2013; 61:91-103; PMID:22653784; <http://dx.doi.org/10.1002/glia.22363>
- [24] Li H, Zhang Z, Zhou X, Wang Z, Wang G, Han Z. Effects of microRNA-143 in the differentiation and proliferation of bovine intramuscular preadipocytes. *Mol Biol Rep* 2011; 38:4273-80; PMID:21113671; <http://dx.doi.org/10.1007/s11033-010-0550-z>
- [25] Li R, Zhang L, Jia L, Duan Y, Li Y, Wang J, Bao L, Sha N. MicroRNA-143 targets Syndecan-1 to repress cell growth in melanoma. *PLoS One* 2014; 9:e94855; PMID:24722758; <http://dx.doi.org/10.1371/journal.pone.0094855>
- [26] Borralho PM, Simoes AE, Gomes SE, Lima RT, Carvalho T, Ferreira DM, Vasconcelos MH, Castro RE, Rodrigues CM. miR-143

- overexpression impairs growth of human colon carcinoma xenografts in mice with induction of apoptosis and inhibition of proliferation. *PLoS One* 2011; 6:e23787; PMID:21901135; <http://dx.doi.org/10.1371/journal.pone.0023787>
- [27] Jordan SD, Kruger M, Willmes DM, Redemann N, Wunderlich FT, Bronneke HS, Merkwirth C, Kashkar H, Olkkonen VM, Bottger T, et al. Obesity-induced overexpression of miRNA-143 inhibits insulin-stimulated AKT activation and impairs glucose metabolism. *Nat Cell Biol* 2011; 13:434-46; PMID:21441927; <http://dx.doi.org/10.1038/ncb2211>
- [28] Sharma A, Hu XT, Napier TC, Al-Harthi L. Methamphetamine and HIV-1 Tat down regulate beta-catenin signaling: implications for methamphetamine abuse and HIV-1 co-morbidity. *J Neuroimmune Pharmacol* 2011; 6:597-607; PMID:21744004; <http://dx.doi.org/10.1007/s11481-011-9295-2>
- [29] Talloczy Z, Martinez J, Joset D, Ray Y, Gacser A, Toussi S, Mizushima N, Nosanchuk JD, Goldstein H, Loike J, et al. Methamphetamine inhibits antigen processing, presentation, and phagocytosis. *PLoS Pathog* 2008; 4:e28; PMID:18282092; <http://dx.doi.org/10.1371/journal.ppat.0040028>
- [30] Lee J, Hur J, Lee P, Kim JY, Cho N, Kim SY, Kim H, Lee MS, Suk K. Dual role of inflammatory stimuli in activation-induced cell death of mouse microglial cells. Initiation of two separate apoptotic pathways via induction of interferon regulatory factor-1 and caspase-11. *J Biol Chem* 2001; 276:32956-65; PMID:11402054; <http://dx.doi.org/10.1074/jbc.M104700200>
- [31] Lee P, Lee J, Kim S, Lee MS, Yagita H, Kim SY, Kim H, Suk K. NO as an autocrine mediator in the apoptosis of activated microglial cells: correlation between activation and apoptosis of microglial cells. *Brain Res* 2001; 892:380-5; PMID:11172787; [http://dx.doi.org/10.1016/S0006-8993\(00\)03257-1](http://dx.doi.org/10.1016/S0006-8993(00)03257-1)
- [32] Rabinowitz JD, White E. Autophagy and metabolism. *Science* 2010; 330:1344-8; PMID:21127245; <http://dx.doi.org/10.1126/science.1193497>
- [33] Hanahan D, Weinberg RA. Hallmarks of cancer: the next generation. *Cell* 2011; 144:646-74; PMID:21376230; <http://dx.doi.org/10.1016/j.cell.2011.02.013>
- [34] Saiki S, Sasazawa Y, Imamichi Y, Kawajiri S, Fujimaki T, Tanida I, Kobayashi H, Sato F, Sato S, Ishikawa K, et al. Caffeine induces apoptosis by enhancement of autophagy via PI3K/Akt/mTOR/p70S6K inhibition. *Autophagy* 2011; 7:176-87; PMID:21081844; <http://dx.doi.org/10.4161/auto.7.2.14074>
- [35] Aoki H, Takada Y, Kondo S, Sawaya R, Aggarwal BB, Kondo Y. Evidence that curcumin suppresses the growth of malignant gliomas in vitro and in vivo through induction of autophagy: role of Akt and extracellular signal-regulated kinase signaling pathways. *Mol Pharmacol* 2007; 72:29-39; PMID:17395690; <http://dx.doi.org/10.1124/mol.106.033167>
- [36] Ellington AA, Berhow MA, Singletary KW. Inhibition of Akt signaling and enhanced ERK1/2 activity are involved in induction of macroautophagy by triterpenoid B-group soyasaponins in colon cancer cells. *Carcinogenesis* 2006; 27:298-306; PMID:16113053; <http://dx.doi.org/10.1093/carcin/bgi214>
- [37] Klionsky DJ, Cuervo AM, Seglen PO. Methods for monitoring autophagy from yeast to human. *Autophagy* 2007; 3:181-206; PMID:17224625; <http://dx.doi.org/10.4161/auto.3678>
- [38] Kroemer G, Galluzzi L, Vandenabeele P, Abrams J, Alnemri ES, Baehrecke EH, Blagosklonny MV, El-Deiry WS, Golstein P, Green DR, et al. Classification of cell death: recommendations of the Nomenclature Committee on Cell Death 2009. *Cell Death Differ* 2009; 16:3-11; PMID:18846107; <http://dx.doi.org/10.1038/cdd.2008.150>
- [39] Klionsky DJ, Abdalla FC, Abeliovich H, Abraham RT, Acevedo-Arozena A, Adeli K, Agholme L, Agnello M, Agostinis P, Aguirre-Ghiso JA, et al. Guidelines for the use and interpretation of assays for monitoring autophagy. *Autophagy* 2012; 8:445-544; PMID:22966490; <http://dx.doi.org/10.4161/auto.19496>
- [40] Zalckvar E, Berissi H, Mizrachy L, Idelchuk Y, Koren I, Eisenstein M, Sabanay H, Pinkas-Kramarski R, Kimchi A. DAP-kinase-mediated phosphorylation on the BH3 domain of beclin 1 promotes dissociation of beclin 1 from Bcl-XL and induction of autophagy. *EMBO Rep* 2009; 10:285-92; PMID:19180116; <http://dx.doi.org/10.1038/embor.2008.246>
- [41] Wirawan E, Lippens S, Vanden Berghe T, Romagnoli A, Fimia GM, Piacentini M, Vandenabeele P. Beclin1: a role in membrane dynamics and beyond. *Autophagy* 2012; 8:6-17; PMID:22170155; <http://dx.doi.org/10.4161/auto.8.1.16645>
- [42] Li DD, Wang LL, Deng R, Tang J, Shen Y, Guo JF, Wang Y, Xia LP, Feng GK, Liu QQ, et al. The pivotal role of c-Jun NH2-terminal kinase-mediated Beclin 1 expression during anticancer agents-induced autophagy in cancer cells. *Oncogene* 2009; 28:886-98; PMID:19060920; <http://dx.doi.org/10.1038/ncr.2008.441>
- [43] Zhang F, Li Y, Tang Z, Kumar A, Lee C, Zhang L, Zhu C, Klotzschewon Ameln A, Wang B, Gao Z, et al. Proliferative and survival effects of PUMA promote angiogenesis. *Cell Rep* 2012; 2:1272-85; PMID:23122957; <http://dx.doi.org/10.1016/j.celrep.2012.09.023>
- [44] Gilmore TD. Introduction to NF-kappaB: players, pathways, perspectives. *Oncogene* 2006; 25:6680-4; PMID:17072321; <http://dx.doi.org/10.1038/sj.onc.1209954>
- [45] Jeffers JR, Parganas E, Lee Y, Yang C, Wang J, Brennan J, MacLean KH, Han J, Chittenden T, Ihle JN, et al. Puma is an essential mediator of p53-dependent and -independent apoptotic pathways. *Cancer Cell* 2003; 4:321-8; PMID:14585359; [http://dx.doi.org/10.1016/S1535-6108\(03\)00244-7](http://dx.doi.org/10.1016/S1535-6108(03)00244-7)
- [46] Villunger A, Michalak EM, Coultas L, Mullauer F, Bock G, Ausserlechner MJ, Adams JM, Strasser A. p53- and drug-induced apoptotic responses mediated by BH3-only proteins puma and noxa. *Science* 2003; 302:1036-8; PMID:14500851; <http://dx.doi.org/10.1126/science.1090072>
- [47] Maiuri MC, Zalckvar E, Kimchi A, Kroemer G. Self-eating and self-killing: crosstalk between autophagy and apoptosis. *Nat Rev Mol Cell Biol* 2007; 8:741-52; PMID:17717517; <http://dx.doi.org/10.1038/nrm2239>
- [48] White E. Deconvoluting the context-dependent role for autophagy in cancer. *Nat Rev Cancer* 2012; 12:401-10; PMID:22534666; <http://dx.doi.org/10.1038/nrc3262>
- [49] Ma J, Wan J, Meng J, Banerjee S, Ramakrishnan S, Roy S. Methamphetamine induces autophagy as a pro-survival response against apoptotic endothelial cell death through the Kappa opioid receptor. *Cell Death Dis* 2014; 5:e1099; PMID:24603327; <http://dx.doi.org/10.1038/cddis.2014.64>
- [50] Chen X, Guo X, Zhang H, Xiang Y, Chen J, Yin Y, Cai X, Wang K, Wang G, Ba Y, et al. Role of miR-143 targeting KRAS in colorectal tumorigenesis. *Oncogene* 2009; 28:1385-92; PMID:19137007; <http://dx.doi.org/10.1038/ncr.2008.474>
- [51] Ouyang YB, Xu L, Lu Y, Sun X, Yue S, Xiong XX, Giffard RG. Astrocyte-enriched miR-29a targets PUMA and reduces neuronal vulnerability to forebrain ischemia. *Glia* 2013; 61:1784-94; PMID:24038396; <http://dx.doi.org/10.1002/glia.22556>
- [52] Chen X, Liu J, Feng WK, Wu X, Chen SY. MiR-125b protects against ethanol-induced apoptosis in neural crest cells and mouse embryogenesis by targeting Bak 1 and PUMA. *Exp Neurol* 2015; 271:104-11; PMID:26024858; <http://dx.doi.org/10.1016/j.expneurol.2015.04.026>
- [53] Xin M, Small EM, Sutherland LB, Qi X, McAnally J, Plato CF, Richardson JA, Bassel-Duby R, Olson EN. MicroRNAs miR-143 and miR-145 modulate cytoskeletal dynamics and responsiveness of smooth muscle cells to injury. *Genes Dev* 2009; 23:2166-78; PMID:19720868; <http://dx.doi.org/10.1101/gad.1842409>
- [54] Prosser HM, Koike-Yusa H, Cooper JD, Law FC, Bradley A. A resource of vectors and ES cells for targeted deletion of microRNAs in mice. *Nat Biotechnol* 2011; 29:840-5; PMID:21822254; <http://dx.doi.org/10.1038/nbt.1929>
- [55] Hu G, Zhou R, Liu J, Gong AY, Chen XM. MicroRNA-98 and let-7 regulate expression of suppressor of cytokine signaling 4 in biliary epithelial cells in response to *Cryptosporidium parvum* infection. *J Infect Dis* 2010; 202:125-35; PMID:20486857; <http://dx.doi.org/10.1086/653212>
- [56] Yao H, Ma R, Yang L, Hu G, Chen X, Duan M, Kook Y, Niu F, Liao K, Fu M, et al. MiR-9 promotes microglial activation by targeting MCP1. *Nat Commun* 2014; 5:4386; PMID:25019481
- [57] Guo WJ, Zhang YM, Zhang L, Huang B, Tao FF, Chen W, Guo ZJ, Xu Q, Sun Y. Novel monofunctional platinum (II) complex Mono-Pt induces apoptosis-independent autophagic cell death in human ovarian carcinoma cells, distinct from cisplatin. *Autophagy* 2013; 9:996-1008; PMID:23580233; <http://dx.doi.org/10.4161/auto.24407>